REVIEW

Multidimensional Architectures for Functional Optical Devices

By *Kevin A. Arpin, Agustin Mihi, Harley T. Johnson, Alfred J. Baca, John A. Rogers, Jennifer A. Lewis,* and *Paul V. Braun**

Materials exhibiting multidimensional structure with characteristic lengths ranging from the nanometer to the micrometer scale have extraordinary potential for emerging optical applications based on the regulation of light–matter interactions via the mesoscale organization of matter. As the structural dimensionality increases, the opportunities for controlling light–matter interactions become increasingly diverse and powerful. Recent advances in multidimensional structures have been demonstrated that serve as the basis for three-dimensional photonic-bandgap materials, metamaterials, optical cloaks, highly efficient low-cost solar cells, and chemical and biological sensors. In this Review, the state-of-the-art design and fabrication of multidimensional architectures for functional optical devices are covered and the next steps for this important field are described.

1. Introduction

Materials exhibiting designed multidimensional architectures have extraordinary potential for emerging optical applications due to their ability to interact with light in ways that cannot be achieved using simple, nonstructured materials. Fundamentally, the introduction of microstructure with characteristic dimensions similar to the wavelength of light can dramatically modulate light–matter interactions. A simple example is a 1D periodic dielectric stack; such a structure can be designed to be resonant with a specific frequency of light, greatly increasing the interaction of the materials comprising the structure with that frequency. Increasing dimensionality to two and three dimensions provides opportunities for far more exotic optical properties including 3D photonic bandgaps, metamaterials, optical cloaking, highly efficient solar cells, and unique sensors. Significant challenges remain including discovery of methods to fabricate multidimensional architectures at fine length scales compatible with a diverse array of materials, development of efficient computational modeling tools, and approaches to electrically and optically interface functional elements embedded within multidimensional architectures with the outside world.

Materials that posses a refractive-index contrast periodically organized on the order of the wavelength of light (known as photonic crystals) strongly modulate light of certain frequencies. For the special case of high-refractive-index-contrast structures containing the proper internal 3D periodic arrangement of matter, a complete photonic bandgap (cPBG) can emerge.[1] Inside a material possessing a cPBG the optical density of states over a certain photon-energy range is zero for all directions. Any infinite dielectric structure with a micrometer-scale periodic refractive-index modulation, however, will exhibit a photonic bandgap (PBG) in at least one specific direction. A good example of such a structure is the aforementioned dielectric stack. A 3D structure alone is not sufficient to generate a cPBG. Structures that have a low-refractive-index contrast, non-optimal periodic structures, or inappropriate 3D structures do not possess cPBG. However, for many applications, a directionally specific PBG (often termed a stop band) is all that is required; therefore, one should not unnecessarily fixate on obtaining a cPBG. Proposed applications for PBG and cPBG materials are quite diverse, and include lossless mirrors, the enhancement or inhibition of emission from embedded emitters,[2] zero-threshold lasers,[3] low-loss 3D micrometer-scale optical waveguides,[4–6] optical circuitry, enhancement of optical absorption processes in solar cells, and sensors.[1]

Since the pioneering work of Yablonovitch[3] and John[7] a majority of research on photonic crystals has been performed on 2D rather than 3D structures. 2D structures have a number of practical advantages, including ease of fabrication using conventional lithographic approaches, clear characterization protocols, and straightforward modeling. However, 2D photonic crystals have a critical limitation, namely that they have limited control over out-of-plane light. More broadly, the ability to completely control the emission and propagation of light within a structure could significantly contribute to the development of transformative optical devices.

Noda has suggested four significant challenges that need to be addressed for 3D cPBG materials to be realized as potential optical devices.[8] First, microstructures with a broad cPBGs in the visible and near-infrared (NIR) need to be fabricated. A broad

[*] Prof. P. V. Braun, K. A. Arpin, Dr. A. Mihi, Prof. H. T. Johnson, A. J. Baca, Prof. J. A. Rogers, Prof. J. A. Lewis
Frederick Seitz Materials Research Laboratory
104 South Goodwin Ave
Urbana, IL 61801 (USA)
E-mail: pbraun@illinois.edu

DOI: 10.1002/adma.200904096

cPBG is of interest because a narrow cPBG is likely to close in a real system due to experimental variability. The first cPBG material, which operated in the microwave regime, was reported in 1991 by Yablonovitch et al.[9] Since then, the characteristic length scale of the dielectric periodicity has been scaled down to the sub-micrometer range with nanometer control of feature location, resulting in materials with cPBGs in the visible and NIR regime.[10] However, significant work remains to demonstrate the reproducibility and manufacturability of these materials. Second, precise control over the placement of defects within a cPBG structure is essential. For example, line defects can serve as low-loss waveguides for light that otherwise would not be able to propagate through the cPBG crystal. Point defects are equally important when coupled with embedded emitters to demonstrate and exploit spontaneous emission inhibition. Third, active emitters or absorbers need to be locally embedded within, or near, a designed defect mode inside the 3D structure. Fourth, electronic grade semiconducting photonic crystals would be required for many actual device applications. For multidimensional photonic structures to achieve their ultimate potential, these challenges must be met. An important component of this Review will be to relate recent advances in a variety of photonic architectures to the aforementioned challenges. A particular area of need is the reproducible fabrication of photonic architectures exhibiting the desired optical properties over a specific frequency range, especially at wavelengths in the visible and near IR, where the design tolerances become very small. The fabrication of controlled defects within such structures is often necessary for device applications and the current state-of-the-art will be presented. Active optical devices, where the photonic crystal enhances light–matter interactions will also be covered. The eventual goal is the fabrication of multidimensional photonic structures with high electronic quality, opening new possibilities for light-based technologies.

2. Fabrication of Multidimensional Photonic Structures

As a consequence of the absence of a Bohr radius for photons, the optical features exhibited by photonic structures are length scale invariant. As a result, structures which are easy to fabricate in the mid-IR become much more challenging to fabricate in the visible and near-IR regions of the electromagnetic spectrum. Through recent advances in the design and fabrication techniques it appears that developments such as a cPBG or optical cloaking may be realizable, even at visible frequencies, although considerable work remains.

2.1. Design and Fabrication of Photonic Crystals

2.1.1. Design and Optimization of Photonic Crystals

The design of a photonic crystal typically starts with a calculation of the band structure for a given geometry and materials composition. Minor variations of the lattice parameter, filling fraction, topology, and refractive indices of the structure are then used to tune the band structure to obtain desired optical properties. However, an approach to solve the inverse problem is much more interesting. Ideally, one would start with the desired optical response and then determine the ideal structure and materials to realize these properties within the physical experimental constraints. For example, the dielectric constant of the structure cannot exceed that of known materials. Physically, it must be possible to fabricate the structure, a constraint that will vary depending on the structure. One powerful approach being actively considered to solve such an inverse problem is based on genetic algorithms (GAs).[11–14] GAs possess a unique ability to find optimal or nearly optimal solutions to problems given a complex multiparameter set of inputs. The weight applied to each input of the problem, for example ease of fabrication, can be varied, providing realistic experimental constraints. In context of multidimensional photonic structures, GAs are especially powerful for holographic fabrication techniques, where the intensity, direction, and polarization of the patterning beams can be independently varied, resulting in a nearly infinite number of possible structures.[15] Through a GA approach, optimized beam configurations for a given multidimensional structure can be determined. Either a known structure can be used to define the fitness of the beam configuration or, when possible, the optical properties of these structures can be used to define the fitness of the overall structure. Examples of possible structural goals with photonic potential include chiral spiral-like structures and diamond-like structures. Large photonic band gaps and other interesting optical properties can also be used as targets. Furthermore, GAs can be used as a computational method to define the structure of a phase mask for proximity field nanopatterning (PnP) of photonic crystals (described in more detail later). As long as the fitness of the resultant structure as a function of the phase mask can be determined, a GA approach is applicable. No advance knowledge of the phase mask design is needed.[16] A GA method, however, is not perfect. If the input parameters are not properly selected, or the fitness function improperly weighted, the result may not be a close match with the desired result.

While fabrication error often has deleterious effects on device geometries such as waveguides, Johnson showed how small deviations from perfect periodicity in some photonic crystal structures, even as a result of random disorder, can lead to performance improvements.[17] This observation leads to a design strategy based on topology optimization. Work first done on waveguide-bend and waveguide-termination geometries shows that substantial improvements can be obtained in realistic devices by use of inverse computational methods.[18,19] It is perhaps not surprising that at points in the structure where symmetry is broken, such as at a bend or surface, deviation from periodicity in the photonic crystal can be beneficial. The concept of topology optimization can also be applied to improve 3D photonic-crystal-based devices such as those described above. In the topology-optimization approach, calculations determine the placement of dielectric material in nonperiodic and irregular topologies; this is illustrated in Figure 1 for the computation-based experimental design of a photonic-crystal laser cavity.[20] In this work, the use of irregular features nearest to the micro-optical cavity boosts the optical confinement, and thus the laser cavity quality factor, by approximately 50%. The calculation is 3D,

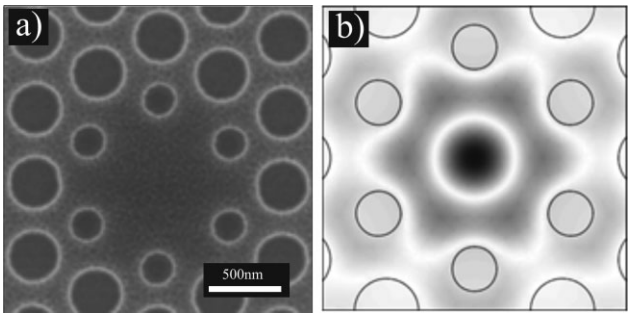

Figure 1. a) SEM image of a cavity embedded in a 2D photonic crystal (courtesy of Johnson and co-workers). b) Simulated spatial distribution of the H_z field in this structure at a resonant-mode frequency. Adapted with permission from [20]. Copyright 2008, American Institute of Physics.

although the device geometry is only allowed to vary in the plane of the photonic crystal. This work has led to a general computational approach for the inverse design of 2D and 3D nanophotonic device elements,[20,21] where a gradient-based design sensitivity analysis is coupled with a continuum solution of the frequency domain wave optics problem, and iteration is carried out over all possible distributions of dielectric material toward an improvement in some device performance characteristic.

2.1.2. Fabrication of Photonic Crystals

The inverse computational methods described above will likely result in complex, multidimensional architectures that will be difficult or impossible to fabricate via traditional methods. Here we will discuss both traditional and emerging fabrication routes and outline where more advanced techniques may be needed, beginning with simple 1D architectures such as distributed Bragg reflectors. Traditionally a Bragg mirror is fabricated by the alternate deposition of dense layers of alternating refractive indices; these structures behave as virtually lossless and highly efficient mirrors over the range of wavelengths where the condition for Bragg diffraction is fulfilled.[22] An emerging area of interest is in porous Bragg stacks. Such 1D structures have become of interest due to the potential to flow materials through the Bragg structure, thus facilitating their use within, for example, dye-sensitized solar devices and chemical sensors.[23,24] Porous Bragg reflectors are obtained by the alternating deposition of densely packed nanoparticle layers composed of materials including SiO_2, TiO_2, and SnO_2,[25,26] clays,[27] or mesoporous films.[28] The dielectric contrast can be achieved either by the use of different oxides for each layer or by varying the porosity of even the same material in different layers.[29] The permeability of these multilayers can be used to allow the flow of chemicals through the structures either to induce a detectable change in optical properties or to enable the efficient photochemical conversion of molecules with the structure. This and other applications of these dielectric mirrors will be examined further in Section 4 of this Review.

Moving beyond 1D, a number of advanced fabrication techniques for multidimensional photonic crystals have been comprehensively discussed elsewhere,[30] and thus the focus here will be on the most recent developments. Figure 2 presents scanning electron microscopy (SEM) images of the typical structures fabricated using some of the most common methods, including colloidal crystallization[31–33] (Fig. 2a),[32] conventional lithography[34,35] (Fig. 2b), direct writing [36–38] (Fig. 2c), and interference lithography[39,40] (Fig. 2d,e). Along with these methods, which are widely used, a number of other fabrication techniques have been demonstrated for 3D photonic crystals including micromanipulation, glancing-angle deposition, electrochemical etching, and X-ray lithography.[30,41]

Colloidal self-assembly is the simplest, and most widely utilized approach to form photonic crystals.[31] It is attractive because of its low cost, ease, and generally good reproducibility. The optical properties of self-assembled colloidal crystals, as measured by the normal incidence reflection, still rival or exceed photonic crystals formed via much more complex methods. The colloids used have primarily consisted of silica, polystyrene, or polymethylmethacrylate spheres ranging from a few 100 nanometer to a few micrometer in diameter. Upon sedimentation or convective assembly of these particles, colloidal crystals can be formed containing anywhere from a few to hundreds of layers.[42] In an effort to increase the effective photonic strength, colloidal crystals are typically utilized as sacrificial templates for the

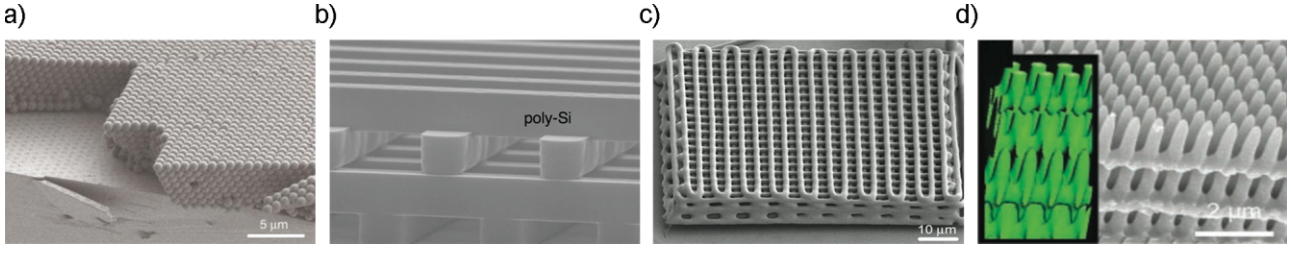

Figure 2. SEM images corresponding to 3D photonic crystals obtained by different fabrication procedures. a) Colloidal crystallization by evaporation-induced self assembly. Reproduced with permission from [33]. Copyright 2001, Macmillan Publishers Ltd. b) Conventional lithograpy. The structure is fabricated by repeating silica deposition, patterning, etching, silicon deposition, and polishing steps. Reproduced with permission from [35]. Copyright 1998, Macmillan Publishers Ltd. c) Direct ink writing. A concentrated polyelectrolyte ink is dispensed through a nozzle attached to a three-axis (*x*,*y*,*z*) micropositioning device. Reproduced with permission from [61]. Copyright 2004, Macmillan Publishers Ltd. d) Interference lithography. The inset represents the corresponding computed optical intensity distribution. Reproduced with permission from [40]. Copyright 2004, National Academy of Sciences, USA.

deposition of high-refractive-index materials such as Si, GaAs, InP, Ge, or TiO_2. Over the past few years, approaches to deposit such materials within a 3D sacrificial template have increased significantly. These and similar materials can now be deposited using chemical vapor deposition,[43] atomic layer deposition,[44] and sol–gel[45,46] or electrodeposition[47] methods. Properly prepared inverted structures are mechanically stable and can exhibit excellent optical properties including even possibly a cPBG.[48] Very recently, to avoid the inversion process, it has been demonstrated that high-refractive-index-contrast silicon-based photonic crystals can be formed by converting a silica opal into a silicon opal with magnesium at 650 °C. The structure of the resulting silicon opal is quite similar to the starting silica structure.[49]

Colloidal self-assembly however results in a periodic structure containing a high density of defects inherent to the assembly process that can dramatically reduce the optical strength. An additional serious shortcoming of colloidal assembly-based fabrication is that all attempts to form crystal structures other than FCC have resulted in very small structures (compared to self-assembly) with weak optical properties.[50] Unfortunately, FCC, the easiest to obtain structure, is not ideal for most applications. Non-FCC structure created to date include the use of a nanorobot to fabricate a diamond structure using colloidal microspheres of silica and polystyrene, as demonstrated by Garcia-Santamaria et al.[51] Benito et al. used computer-controlled holographic optical tweezers to fabricate various FCC and simple cubic structures.[52] If colloidal crystallization is to find real applications beyond simple proof-of-concept experiments, lage-scale, high-quality colloidal crystals with structures other than FCC need to be realized. Hynninen et al. recently proposed a potential solution to these problems based on a self-assembly technique that could potentially produce large-scale, high-quality, diamond-structured colloidal crystals.[53] Following this approach, a diamond structure could be formed using spheres of two different sizes and types. in the appropriate concentrations, followed by the selective removal of one type of sphere. The resulting diamond structure is predicted to have powerful optical properties if comprised of spheres of high dielectric constant.

Powerful optical properties may be obtained from colloidal fabrication techniques if disorder in the structures is actually promoted, rather than minimized. Randomly arranged spherical colloid films are being investigated as photonic glasses.[54] These structures exhibit interesting phenomena including light localization and random lasing.[55,56] Two fabrication routes have been followed to obtain such ''glasses''. Either, electrolyte can be introduced in small amounts into the colloidal dispersion encouraging colloidal aggregation, or two different types of colloid can be co-assembled, followed by selective etching of one type of colloid to yield the desired ''glass''.

Conventional 2D lithography techniques highly developed by the semiconductor industry can be applied to fabricate 3D photonic structures, however, with considerable cost. Photo and/or electron-beam lithography can be used to define a 2D pattern in a photoactive material (photoresist); this pattern can then be transferred to a high-refractive-index material via conventional etching protocols. These processes can be repeated numerous times to generate the 3D structure.[34,35] Major challenges remain for layer-by-layer registration and retention of good electronic properties. These 2D technologies require excessive time and effort to assemble 3D architectures. The remainder of this section will examine, in greater detail, two promising approaches to the fabrication of 3D photonic crystals.

Direct-write processes have been widely applied to complex 3D photonic-crystal structures. Two common and complementary variants of the direct-write process are multiphoton direct laser writing and direct ink writing. As reviewed by Fourkas and co-workers, in the former, direct laser writing, a highly focused laser beam is translated in a designed pathway through a negative photoresist, generating, with submicrometer accuracy, a defined 3D structure.[57,58] This technique has been employed to generate a variety of multidimensional photonic microstructures (Fig. 3) with interesting optical properties. In the latter, direct ink writing, ink with tailored rheological properties is extruded through a fine nozzle, which translates into a computer-controlled 3D pattern. As Lewis has demonstrated, the ink can be based on organic, inorganic, or combinations of organic and inorganic materials.[59–62] The key requirement is that the ink has a sufficiently high shear elastic modulus to span across gaps, while not clogging the nozzle. Very fine structures have been realized by patterning both polyelectrolyte and sol–gel inks through a fine nozzle. The sacrificial polymeric structures have been used as templates for silicon and germanium-based photonic crystals,[36,63] while the patterned sol–gel structures have been transformed into high-refractive-index-contrast TiO_2 photonic crystals upon heating at elevated temperatures (400–600 °C).[59] Unlike polymeric periodic microstructures, which need to be inverted or converted into a high-refractive-index material in order to obtain desired optical features and quality,[62] no inversion is needed for the direct-write high-refractive-index

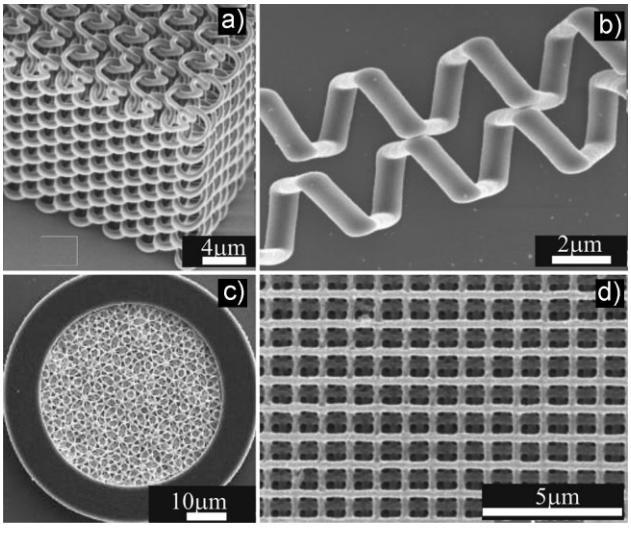

Figure 3. SEM images of complex three-dimensional photonic structures obtained via multiphoton absorption polymerization: a) Spiral photonic crystal with a 180° phase shift between adjacent spirals. b) Close-up view of two individual spirals extracted from the structure. Reproduced from [154]. c) Photonic quasicrystal. Reproduced with permission from [155]. Copyright 2006, Macmillan Publishers Ltd. d) Si photonic crystal created using a double inversion strategy. Reproduced from [38].

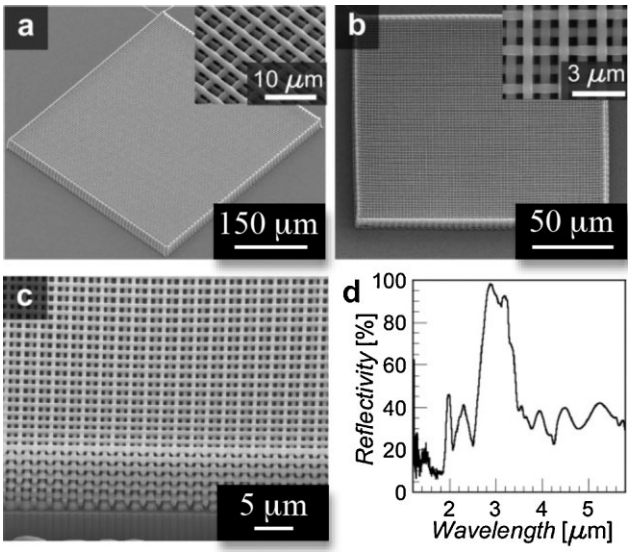

Figure 4. SEM image of a 24-layer, 3D structure fabricated through direct ink writing of a sol–gel based TiO_2 ink a) before and b) after heating at 715 °C. The insets in (a,b) show higher magnification views. c) High-magnification image showing the cross-section of the oxide structure shown in (b). d) Specular reflectance measured from the oxide structure shown in (b). Adapted from [59].

TiO_2 photonic crystals. Following calcination, the desired oxide material is obtained in an organized 3D periodic microstructure exhibiting excellent optical properties (Fig. 4). Reservoir-induced coagulation,[61] solvent evaporation,[59] or photopolymerization in air[64] induce the desired solidification of the cylindrical filaments during direct assembly.

A very promising 3D fabrication technique with the potential to create nearly arbitrarily complex, very-large-area, defect-free 3D photonic crystals is interference lithography. The required 3D interference patterns can be formed inside a photoresist by several methods. In one variant, four or more non-coplanar coherent laser beams are aligned to interfere within a photoresist. In Figure 5a–c different cross-sections of a polymeric 3D structure are shown, obtained with four-beam interference holography. The high quality of these structures is reflected in their optical properties (Fig. 5d).[65,66] In another variant, pioneered by Rogers and co-workers, a 2D elastomeric phase mask is either placed in conformal contact with a photoresist or used to imprint a relief pattern into the top surface of the photoresist (Fig. 6a–c).[40] Upon exposure with a coherent source (Fig. 6d), multiple diffracted beams arise within the photoresist. These multiple beams interfere, generating a 3D periodic intensity distribution within the photoresist, which can be subsequently developed (Fig. 6e–g) in this PnP approach.[40] Following exposure and subsequent development, a high-refractive-index material can be deposited into the photoresist template to obtain a 3D PBG material.

Recently, two-photon PnP-based interference lithography was demonstrated. The two-photon-based photoexcition process results in higher-contrast structures due to the quadratic density dependence of absorption.[67,68] For two-photon exposure, PnP has a substantial advantage over multibeam approaches in that the multiple diffracted beams are necessarily temporally coherent since they are all generated right at the top surface of the photoresist. Achieving temporal coherence for conventional multibeam interference requires very close attention to the path length of the various beams.

Interference lithography is highly attractive because it can be used to fabricate micro architectures that cannot be achieved using other conventional fabrication technologies. For example, functional-density-graded materials can be achieved by altering the spectral bandwidth, the illumination angle, and the degree of collimation of the exposure.[69,70] Alternatively, 3D photonic crystals with unique geometries have been realized by modifying the structure and order of the 2D diffraction grating used for PnP.[67] Finally, uniquely shaped objects can be created via interference lithography.[71,72]

Common polymeric photoresists, such as SU-8, typically exhibit glass-transition temperatures of around 100 °C, complicating the generally high-temperature direct inversion to high-refractive-index materials. Thus, inversion of these structures to high-refractive-index materials usually requires a multistep process where an intermediate layer with high temperature stability is deposited at low temperature followed by the removal of the polymeric photoresist. Finally, the high-refractive-index phase is added. For a number of reasons, this multistep is often undesirable. Braun and co-workers have recently demonstrated the ability to define photonic crystals in an inorganic photoresist using PnP.[72] The silsequioxane-based photoresist is stable up to 500 °C and thus holographic structures can be directly used as templates for materials deposited using high-temperature techniques.

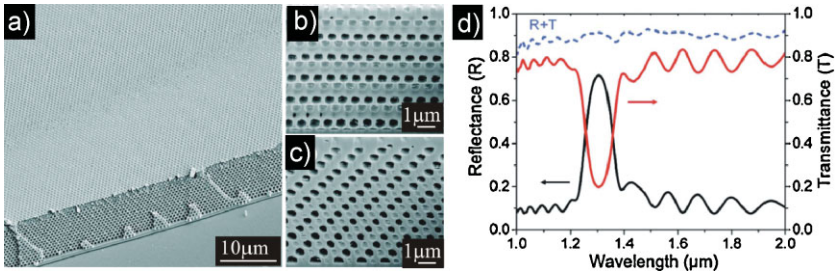

Figure 5. a–c) SEM images of a polymer photonic crystal obtained by four-beam interference holography. d) Reflectance and transmittance spectra of this photonic crystal. Adapted with permission from [66]. Copyright 2007, American Institute of Physics.

2.2. Design and Fabrication of Metamaterials

Electromagnetic metamaterials are structured materials that exhibit properties not commonly found in naturally occurring solids. Typically, they require advanced multidimensional architectures, which are difficult, if not impossible, to fabricate via standard approaches. Realization of the promising applications of metamaterials thus requires advances in multidimensional

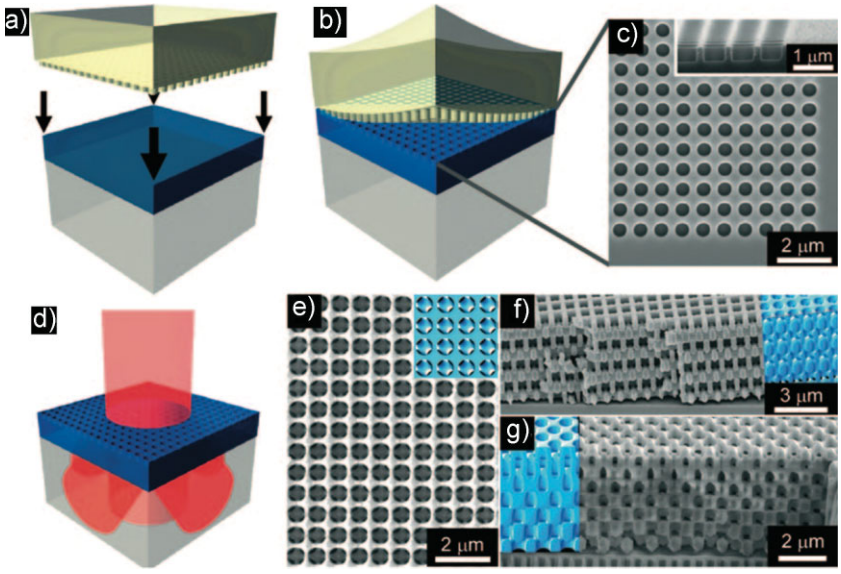

Figure 6. Maskless PnP process for the fabrication of 3D periodic microstructures by imprinting a relief pattern into the topsurface of thephotoresist. a,b) Schematic views of the micromolding process using an elastomeric PDMS stamp. c) SEM image of the relief structure of the micromolded photoresist surface (the inset shows the cross-section). d) Graphical representation of the diffracted beams obtained upon illumination of the surface-patterned photoresist. e–f) SEM images from different crystalline planes found in the 3D photonic crystals obtained with the PnP method. The expected structure according to theoretical simulations is shown in the inset. Adapted from [72].

fabrication techniques. Since Veselago first considered the theoretical existence of materials with negative refractive indices,[73] which he termed left-handed materials, there has been significant work toward realizing these metamaterials for a variety of electromagnetic applications. Several key advances in fabricating materials with both negative permittivity and negative permeability, typically composite materials that would be useful in particular bands of the electromagnetic spectrum,[74,75] have opened up many applications in optics, imaging, telecommunications, sensing, and other areas. Numerous full length reviews have been published recently on this topic, including one in this journal by Soukoulis, which focused in the area of materials science.[76] Here, we briefly discuss several specific areas, in which periodic photonic nanostructures are developed for applications related to negative-index materials.

2.2.1. Negative Refraction with Photonic Structures

Following on the early experimental work on composite materials with negative effective indices, Luo et al. showed, using simple band-structure calculations, that photonic crystals can exhibit all-angle negative refraction in certain frequency ranges, despite having both positive group velocities and positive refractive indices. Such structures have a negative photonic effective mass in these frequency ranges, as predicted by the local curvature of the photonic bands at these frequencies; thus, they still induce negative refraction of beams incident from free-space onto the photonic crystal.[77] Experimental results, obtained using the configuration shown in Figure 7, confirm this for certain classes of photonic crystals in the microwave region.[78] As pointed out by Luo, based on Pendry's work,[79] this effect can be exploited for superlensing, or subwavelength imaging purposes. Cubucku showed this effect in photonic-crystal media, both theoretically and experimentally, opening up a new range of optical applications of periodic photonic nanostructures.[80] Furthermore, the same potential for superlensing applications should be present in 3D structures, including those fabricated by colloidal deposition of inverse opal photonic crystal templates.[81]

2.2.2. Cloaking with Photonic Structures

The mechanism of negative refraction can be harnessed for applications in the emerging area of electromagnetic cloaking, which has received tremendous interest recently.[82] The notion of cloaking through microstructural design has its basis in the observation that a simple coordinate transformation approach can generate a medium in which electromagnetic waves pass around an object into the far field completely undisturbed, relative to the case in which the object is not present. This conformal mapping approach can be rigorously formulated as a design strategy,[83,84] and Smith and co-workers have reported several groundbreaking experimental designs that achieve electromagnetic cloaking in the microwave region of the spectrum (Fig. 8).[85] This design, and others recently reported in the literature, is limited by absorption due to the use of metallic metamaterials and may be difficult to scale down to the visible portion of the electromagnetic spectrum. However, cloaking effects in plasmonic and photonic crystal materials are also possible.[86] Recent work demonstrates that the optical anisotropy and photonic bandgaps attainable with photonic crystals in the visible and near-IR part of the spectrum allow for cloaking effects,[87] even for relatively simple, asymmetric silicon designs (Fig. 9).[88]

Recently, Zhang and co-workers achieved the first experimental demonstration of cloaking at near-visible wavelengths.[89] Following the design obtained with the quasiconformal mapping approach, an optical "carpet" cloak has been fabricated using dielectric materials, thus overcoming the losses limiting metallic metamaterials. The carpet-cloak concept was first introduced by Pendry and co-workers.[90] When placed around an object, this carpet would protect it from interacting with electromagnetic waves, turning it invisible. This new design conceals an object placed within a curved reflecting surface by imitating the reflectance from a flat reflecting surface. To do so, a 2D lattice of cylinders with varying density on a silicon-on-insulator wafer was fabricated through focused-ion-beam milling, and directional electron-beam evaporation was used to deposit 100 nm of gold onto the bump surface. Figure 10 shows a schematic and an SEM image of this optical carpet

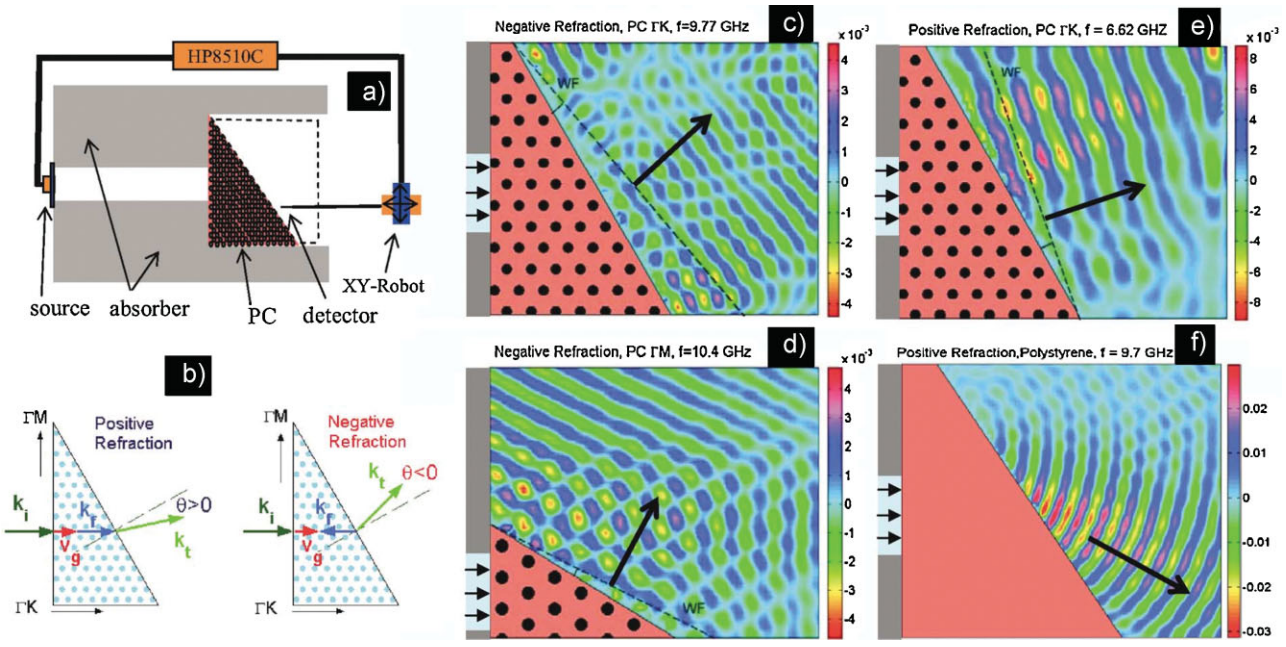

Figure 7. a) Schematic representation of the experimental setup and b) illustrations of the different propagation wave vectors obtained in positive and negative refraction. c–f) Microwave electric-field maps in the far-field region. c) Negative and e) positive refraction by a metallic PC prism along the Γ-K orientation. d) Negative refection for the incident beam along the Γ-M orientation. f) Positive refraction by a polystyrene prism. Reproduced with permission from [78]. Copyright 2004, American Physical Society.

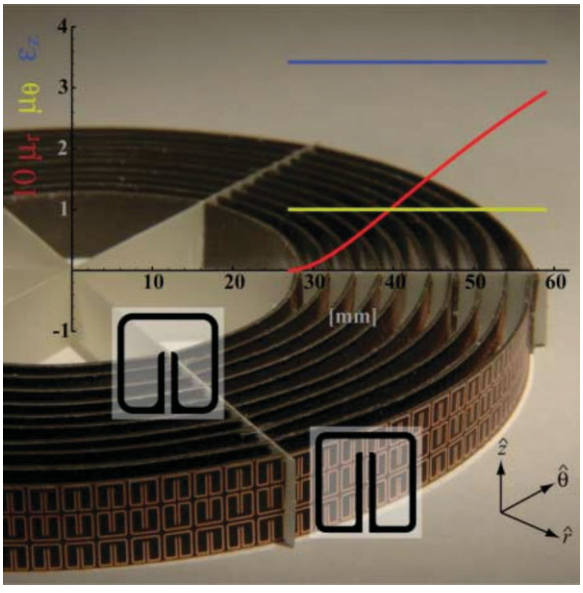

Figure 8. Image of a 2D microwave cloaking structure made of split-ring resonators (insets) positioned with their axes along the radial direction. The graph also represents the material values for the dielectric constant (μ_r) and permeability (ε_z). μ_r (red line) is multiplied by a factor of 10 for clarity. μ_θ (yellow line) has the constant value 1. ε_z (blueline) has the constant value 3.423. Reproduced with permission from [85]. Copyright 2006, American Association for the Advancement of Science.

cloak where the hole array is divided in two regions, one with a uniform pattern and the other with a variable profile. This cloaking device, made of isotropic dielectric materials, enables invisibility over a wide wavelength range (1.4 to 1.8 μm), but extension of these devices into the visible range is limited by the resolution of the fabrication processm, which results in roughness in the structure that unacceptably increases scattering losses at shorter wavelengths.

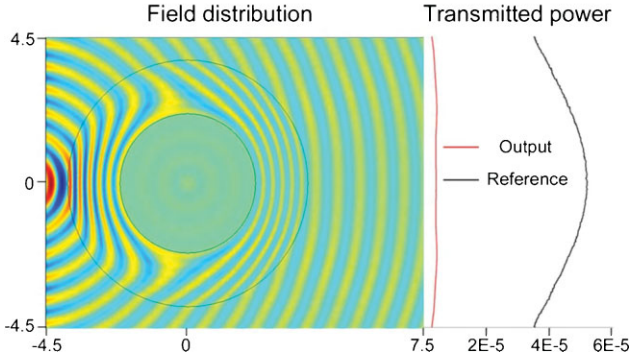

Figure 9. Field and power distribution of a 2D cloaking device with an effective index that follows the ideal formalism, but with an effective conductivity of 500 S m^{-1} under a Gaussian beam illumination of 0.7 μm. The traces on the right represent the transmitted power distribution with (red line) and without (black line) the device. Adapted with permission from 88 Copyright 2008, Optical Society of America.

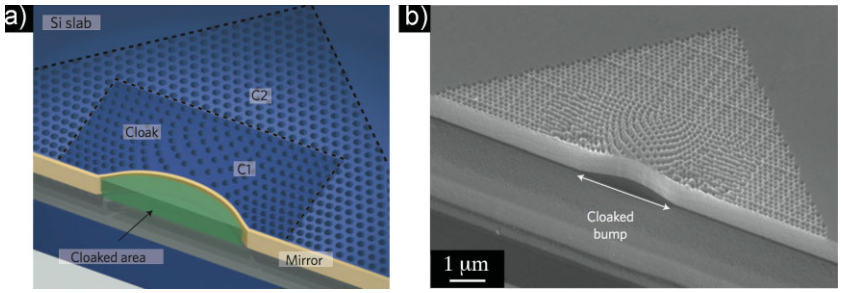

Figure 10. The carpet-cloak design that transforms a mirror with a bump into a virtually flat mirror. a) Schematic diagram of a fabricated carpet cloak. The cloaked region (marked with green) resides below the reflecting bump (carpet) and can conceal any arbitrary object. b) SEM image of a fabricated carpet cloak. The width and depth of the cloaked bump are 3.8 μm and 400 nm, respectively. Reprinted with permission from [89]. Copyright 2009, Macmillan Publishers Ltd.

2.3. Future Directions for Multidimensional Fabrication

There are a number of promising results showing how new inverse computational design approaches and additional developments in 2D and 3D fabrication methods will facilitate further advances in the use of periodic and aperiodic photonic nanostructures. Optimized design routes, which take into consideration limitations in fabrication techniques, are leading to architectures that exhibit interesting optical properties but also are experimentally feasible. The combination of the appropriate design and use of modern lithographic techniques has lead to the first evidence of cloaking in the visible range, opening the door for further promising applications in this field.

3. Multidimensional Defects in PBG Materials

Engineered defects are necessary to realize many proposed applications for PBG materials. Defects within PBG materials can serve to open allowed states otherwise within a photonic bandgap. Light coupled to these defects is strongly localized; the exact nature of the light localization is highly dependent on the size and shape of the defect. An optimal defect fabrication technique exhibits control of the size, shape, and placement of the resultant defect with high precision and, for a number of practical reasons, can even place defects within photonic crystal structures formed via colloidal self-assembly, lithographic techniques, and holography. Direct-write assembly is rather unique in that the photonic crystal and defects can be formed in a single processing step—a significant advantage in some cases.

3.1. Fabrication Techniques

This Review has already discussed fabrication techniques and challenges related to high-optical-quality photonic crystals. As reviewed by Braun a few years ago, the next step in functionalizing photonic crystals is the introduction of defect states within a crystal.[41] Linear defects, which have the potential to confine and guide light through a cPBG crystal, are of interest because of the potential for nearly lossless transmission of light through arbitrarily designed pathways. This type of waveguide may, for example, be advantageous for on-chip optical signal routing, given the potential for small bend radii. Fabrication of such linear defects can either be introduced during the photonic crystal fabrication, for example by the simple omission of rods during woodpile assembly[41] or via multiphoton-based defect writing into a self-assembled structure.[43]

A prime advantage of multiphoton-based defect writing is the possibility to introduce arbitrarily defined 3D defects into a photonic crystal. Inserting a feature into a given layer of a photonic crystal formed via a layer-by-layer process is reasonably straightforward; however, formation of a feature that crosses diagonally through multiple layers is quite difficult. Through the use of two-photon polymerization nearly arbitrary features can be formed.[91] First, a photosensitive monomer system is infilled into the interstitial space of a colloidal crystal. Then, an arbitrary 3D feature is defined by scanning a highly focused intense laser beam in a defined pattern through the material (Fig. 11). To generate the required high-refractive-index contrast, silicon is then infiltrated into the structure by means of chemical vapor deposition (CVD) and the colloidal template is finally removed, resulting in a silicon inverse opal with a clearly defined waveguide. Waveguiding in the IR through these features was observed (Fig. 12).[43] This approach can be applied to photonic-crystal templates formed via other pathways. For example, a similar process was used to embed defects in

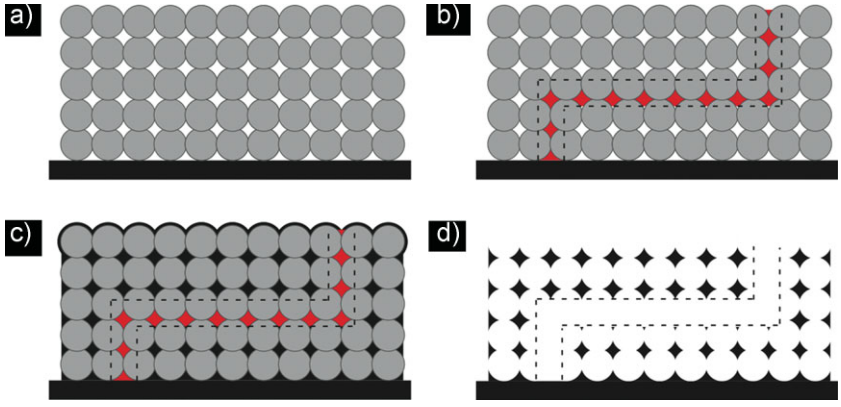

Figure 11. Procedure employed to embed waveguides within silicon inverse opals. a) Silica colloidal crystal grown by convective self assembly and stabilized with a thin alumina layer, b) colloidal crystal with embedded TPP features, c) composite structure obtained after infiltration of silicon through CVD, and d) silicon inverse structure with embedded air defects obtained after removal of oxides and polymer. Reprinted with permission from [43], Copyright 2007, Macmillan Publishers Ltd.

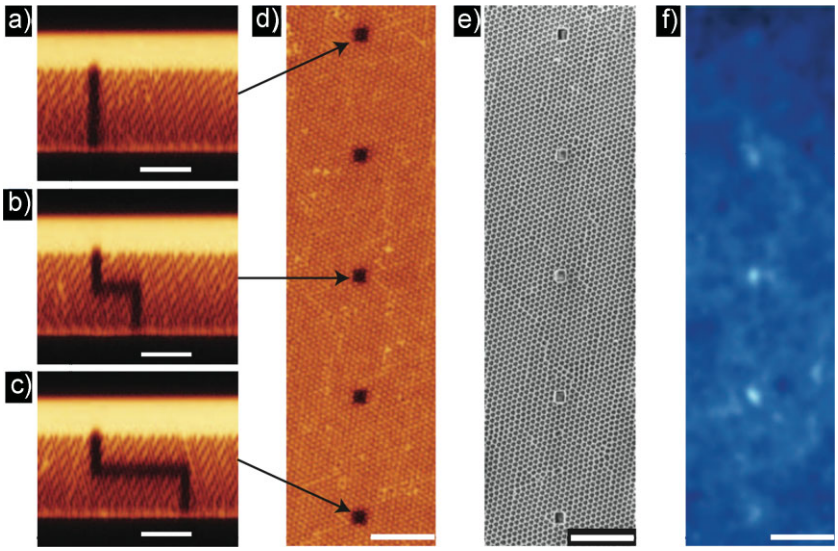

Figure 12. a–c) Laser scanning confocal microscopy images showing various waveguides embedded in a 3D silica photonic crystal from a cross-sectional and d) top view. e) SEM image of the top surface after silicon deposition and removal of the template. f) Infrared microscopy image showing light transmitted through waveguides using a bandpass filter centered at 1.48 mm. Scale bars: 10 μm. The colloidal sphere diameter is 925 nm. Reproduced with permission from [43]. Copyright 2007, Macmillan Publishers Ltd.

holographically defined crystals, however, waveguiding has yet to be observed in such systems.[92]

Registration of any designed defect with the underlying photonic crystal lattice is critical. Not only will it almost certainly be required to have the line defect run from one very specific point to another very specific point, but it may also be interesting to control the interaction of the line defect with other defects present in the photonic crystal. For example, the photonic crystal may contain intentional or unintentional point defects that exhibit optical activity. The coupling of light into and out of carefully designed point defects, which contain optically active materials, would be quite interesting. If a point defect contains an embedded emitter, the line defect could serve as a pathway for the point defect to interact with the outside world. Coupling of light between a waveguide and an optical cavity will only be possible if a procedure exists to place the various features with high precision. Actual device fabrication will require the precise placement of defects not only with respect to each other, but also in relation to the photonic crystal lattice.[93] Multiphoton writing has been at the forefront of this defect technology as well. Careful placement of features adjacent to point defects within self-assembled colloidal crystals has been demonstrated.[94] This is not only significant for device fabrication but also for the optimization of the quality factor (Q-factor) and the resonant frequencies of optical cavities, which have been shown to depend on lattice position.[95]

3.2. Future Directions

Multiphoton writing is a highly flexible and robust technique for writing arbitrary defects within a PBG material. Although significant progress has been made, substantial work remains to realize such structures. Multiphoton writing is a slow, serial fabrication process that will be difficult to scale up, unless exotic optical approaches are applied, the resolution limit of multiphoton writing is on the order of 100 nm, and multiphoton writing is inherently expensive. Clearly, better approaches are needed, but there is every reason to believe ultrahigh-resolution 3D patterning will be possible if appropriate methods and materials are developed.

4. Active Photonic Structures

Periodic photonic structures have been finding application since their initial development. Among those, the most straightforward applications have been those to control light–matter interaction, for example by enhancing the light absorption for a certain material or by inhibiting emission at a certain wavelengths. These properties have enabled more-efficient light extraction from light-emitting diode (LED) structures. Another application for active photonic crystals that has been widely explored is that of sensing, where shifts in the optical properties of functionalized photonic structures can be associated to amounts of a certain molecule or material that is aimed to be detected.

4.1. Emitters Embedded Within Photonic Crystals

Optical emitters embedded within photonic-crystal structures have been of considerable interest from the early days of photonic crystals. 2D photonic crystals have long been suggested for use as microcavities to regulate the emission of light both in and out of the plane. Painter et al. demonstrated a photonic-crystal vertical-cavity surface-emitting laser (VCSEL), in which an in-plane defect mode, matched to the wavelength of the gain medium, is confined by a triangular lattice photonic crystal (PC) structure etched into a suspended heterostructure; partial vertical confinement is due to total internal reflectance.[96] The layout of this device is shown in Figure 13. Various design aspects to enhance the interaction of the emitter with the photonic crystal have been considered by other groups, including variation of the photonic crystal structure in both the lateral direction and the etching direction, which can activate higher defect-mode resonances.[97,98] Considerable effort has also been devoted to improving the performance of the device by locally varying the photonic-crystal geometry. The quality factor of the optical cavity has been shown in computational studies to be strongly modulated by the size of the photonic-crystal features nearest to the cavity region.[99]

Nelson and Braun recently discussed how complete optical confinement will probably require a 3D structure exhibiting a cPBG in order for the most exciting applications to be realized.[2] In 2008, Aoki et al. demonstrated, for the first time, *complete*

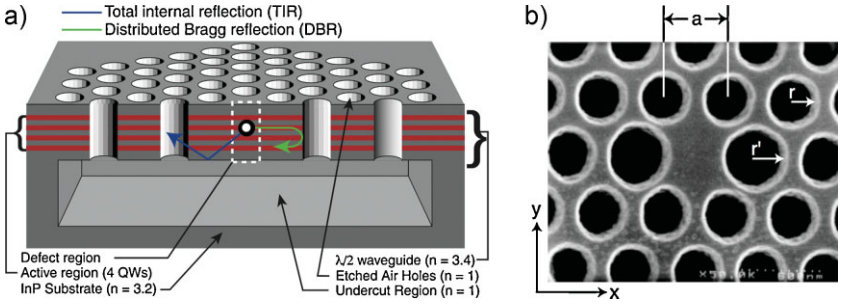

Figure 13. a) Schematic image and b) SEM image of a photonic-crystal microcavity capable of confining light in 3D. The in-plane light localization is obtained by removing a single hole in the 2D photonic crystal. Out-of-plane confinement in the device is achieved via total internal reflection in the low-index cladding. The dimensions are: $a = 515$ nm, $r = 180$ nm and $r' = 240$ nm. Reproduced with permission from [96]. Copyright 1999, American Association for the Advancement of Science.

confinement of emission from quantum dots embedded in an optical cavity.[100] They reported a Q-factor (measure of confinement power) of 2300. This Q-factor was the highest ever reported for a 3D photonic crystal cavity. These high-Q cavities were fabricated by stacking individual planar layers using a micromanipulation technique resulting in a woodpile-like structure. A central layer containing a point defect was doped with InAsSb quantum dots that emit at 1.5 μm. Recently, they increased the Q-factor of their optical cavity to 8600 by increasing the number of stacked layers from 17 to 25 (Fig. 14) and by optimizing the cavity

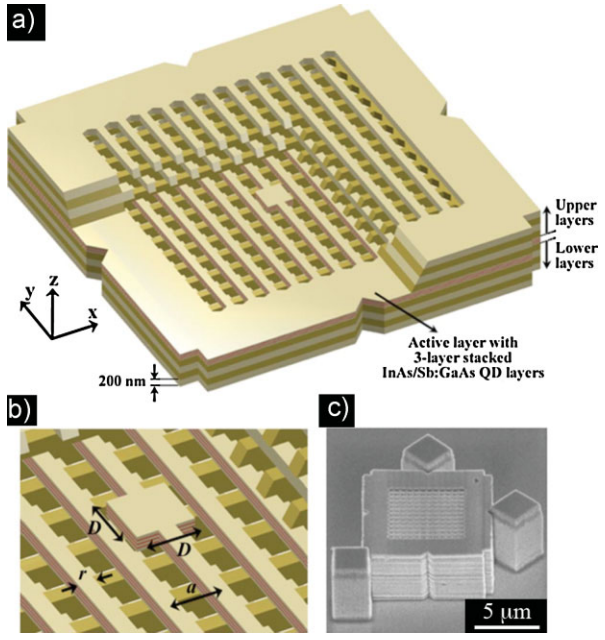

Figure 14. a) Schematic representation of the high-Q 3D photonic crystal assembled using micromanipulation technique. b) Expanded schematic image showing the high-Q nanocavity that was coupled to quantum-dot emitters. $a = 500$ nm, $r = 0.25a$, D represents the size of the defect, which was optimized to obtain the high-Q factor. Reproduced with permission from [101]. Copyright 2009, American Institute of Physics.

size to ensure the cavity mode was in the center of the complete bandgap.[101] Because the individual layers were physically stacked, the overall electrical quality of the structure was presumably low and thus only optical pumping, and not electrical pumping, of emission could be demonstrated. These studies are only the first of what will likely be a series of exciting developments. If electrical pumping can be achieved, it greatly increases the possibility that many of the proposed applications for photonic crystals will become reality.

4.2. Enhanced Light Extraction in LEDs

LEDs are one important application where multidimensional photonic structures can enable dramatic technological advances. Recent advances in both the materials and designs of LEDs have led to dramatic improvements in the overall efficiency. LED efficiency depends primarily on two factors, the efficiency of light generation in the active region of the device, and, as is sometimes underappreciated, the efficiency of coupling light generated in the device and the external world (light extraction). Subwavelength-scale structuring of the device surface is now seen as a viable means to improve efficiency, potentially boosting light extraction by 50% or more. For example, by patterning the top surface of the LED with a 2D photonic crystal, it is possible to significantly reduce losses due to total internal reflection of modes generated in the light-emitting layer, as illustrated in Figure 15a and 15b.[102,103]

Several groups have demonstrated this strategy in practice. Ichikawa and Baba show this enhancement in an epitaxially grown GaInAsP-based LED device with a triangular-lattice 2D photonic-crystal surface grating.[104] Through appropriate design of the photonic crystal geometry, such a structure can be used both to increase light extraction and to tailor the direction of the emission from a LED.[105] Wierer et al. demonstrated that the use of a photonic-crystal layer in GaN LED devices can lead to external efficiencies that are competitive with the best nonphotonic crystal designs.[106] Even simple nanometer-scale roughening of the top surface of the LED increases the extraction efficiency; however, this approach provides only limited control over the direction of the emission. Huang et al. demonstrated this in a GaN LED device, using nanoimprint lithography to create a mask that transfers an etched pattern of 100-nm-scale holes into the SiO_2 surface layer of the device; the output power of the nanoroughened surface is improved by 48% over an otherwise equivalent smooth surface.[107] Through further optimization of the various competing ideas to enhance extraction efficiency, structures could be realized that contain no confined modes as shown in Figure 15c. Such an ideal structure could lead to extraction efficiencies approaching 100%, however in practice such free-standing structures have a number of problems, including thermal-management and charge-transport issues.

It is interesting to consider the effect of adding 3D structure to LEDs. However, unless out-of-plane structuring provides

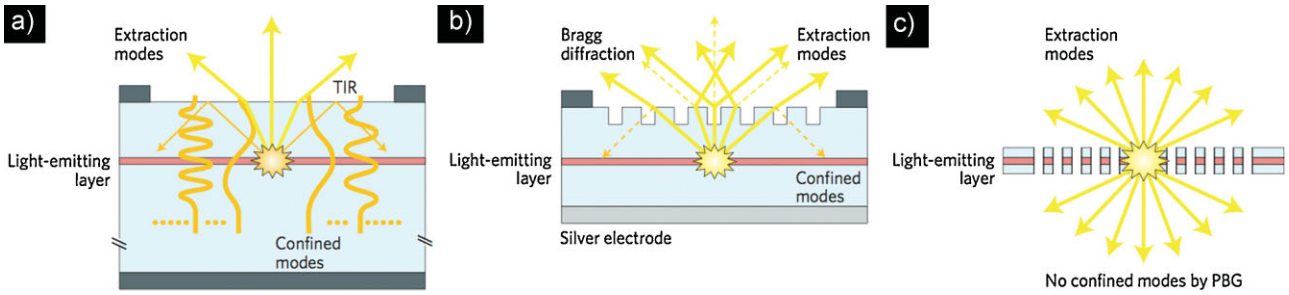

Figure 15. Schematic representations of the pathways for light extraction from a light-emitting layer embedded within a) conventional planar-surface structure, where most of the light is confined inside by total internal reflection at the surface, b) a slab with photonic crystal textured surface, in which some confined modes still exist, and c) the ideal structure, a 2D photonic-crystal slab, where emission into confined modes is inhibited. Reproduced with permission from [102]. Copyright 2009, Macmillan Publishers Ltd.

dramatic improvements in optical extraction without degrading the internal quantum yield, the driving motivation for such structures will be limited by currently available fabrication techniques and, to date, arguments for periodicity in the out-of-plane dimension for a structure are not yet compelling. At minimum, the achievement of electrical contacts to an emissive layer sandwiched within a 3D photonic crystal will be difficult. Assuming this problem can be solved, very careful engineering will be required to create a structure that may not result in substantial improvements in light extraction over that provided by a much simpler 2D structure. However one can imagine that complete control over both the direction and emission wavelength of an LED could provide a substantial advantage over anything possible using a 2D structure, and thus there remains motivation to utilize 3D structures in LEDs.

4.3. Enhanced Absorption in Photonic Structures: Photovoltaics

Solar energy has aroused a great deal of interest in the last years due to the increasing demand for carbon-free energy. However, for solar energy to make a substantial impact to the world's carbon footprint, significant cost reductions and efficiency gains will be necessary. A number of new solar-cell designs are under development with this goal in mind.[108] Existing technologies, such as those based on silicon, are also improved. Here, an overview of various approaches to improve the cost-efficiency ratio of existing solar technologies will be presented, classified according to the element of the photovoltaic (PV)-conversion system that is altered: the absorbing layer, the light concentrator or the incident photon flux. Recent improvements that will be discussed include the use of scattering elements to increase the light-path length and approaches to assemble PV devices from ribbons or discrete pieces of semiconducting materials onto low-cost substrates.

4.3.1. Light Trapping in Solar Cells

Since the earliest stages of their development, PV devices have included elements to maximize the number of photons reaching the active layer without negatively affecting electronic transport within the device. One of the first elements developed was the antireflective coating (ARC). Such a coating consists of a layer of the appropriate thickness (a quarter of the optical length) and a refractive index between that of the cell and the incident medium (usually air), thereby minimizing light reflected from the cell. Although important for all solar cells, the high refractive index of most semiconductors makes ARCs a common component of silicon PV cells. Other common elements used in solar cells to increase the optical path of light include backside mirrors, textured surfaces that randomly scatter light,[109] and surface diffraction gratings. Photonic crystals can also be used to enhance the absorption of the active material through the unique properties that these structures exhibit.[110] For example, photonic crystals can be used as dielectric mirrors at wavelengths where the structures show a photonic bandgap, providing higher reflectivity than their metallic counterparts.

The application of 2D or 3D photonic crystals as a diffraction grating in the interior of a solar cell device, is shown schematically in Figure 16.[111] The diffractive optical properties of 2D photonic crystals, including the effect of surface termination, are well understood theoretically.[112] As such, it is possible to design a photonic-crystal geometry in order to increase the path length of light diffracted from the bottom of the cell back into the thin film absorber layer and thus increase the overall efficiency of the solar cell device. Zhou and Biswas designed such a structure using a computational approach for an amorphous hydrogenated silicon solar cell, in which a 2D photonic-crystal diffraction element is etched into a thin indium tin oxide (ITO) layer on the bottom, which also serves as an electrical contact.[113] Bermel et al. analyzed a similar design for a crystalline silicon cell, and put this design in the context of other wave-optics-based periodic photonic elements, including a distributed Bragg reflector (Fig. 16a), which offers control over only-reflected light, a 2D grating (Fig. 16b), which gives a degree of control over reflected, diffracted, and refracted light, and a 3D photonic crystal (Fig. 16c), which allows complete control over reflected, diffracted, or refracted light passing through the thin-film absorber layer.[111] These designs offer significant potential improvements over geometrical optics-based elements such as high-reflectivity metallic mirrors.

Emerging solar technologies, such as dye-sensitized solar cells (DSSCs), also require the presence of scattering elements to

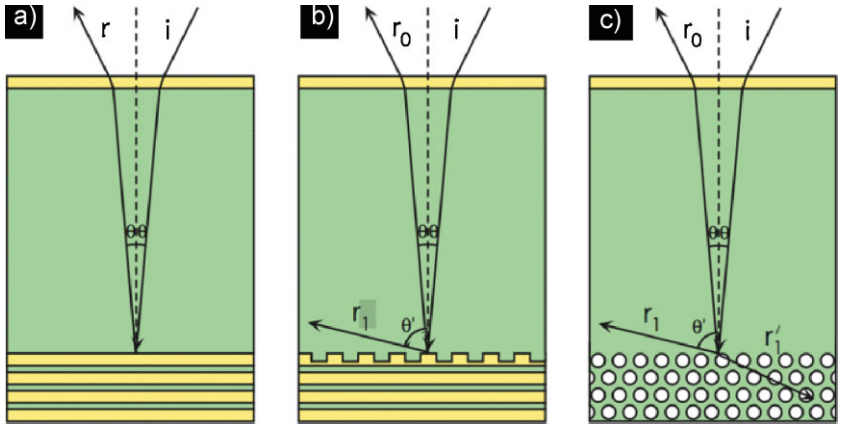

Figure 16. Schematic images showing alternatives to enhance the optical path length of light within a solar cell by coupling to a) a distributed Bragg reflector, b) a DBR plus periodically etched grating, and c) a photonic crystal consisting of a triangular lattice of air holes. Crystalline silicon is depicted in green, low dielectrics in yellow, and air in white. Adapted with permission from [111]. Copyright 2007, Optical Society of America.

enhance the absorption at certain wavelengths. However, few light-enhancing elements have been successfully introduced in those cells due to incompatibilities with the required PV components for DSSCs. These cells have attracted much attention since their first discovery in the 1990s due to their inexpensive components and ease of manufacture.[114] Typically, DSSCs are based on a nanoparticulate titanium oxide electrode sensitized with a ruthenium-based dye, a liquid electrolyte, (typically an iodide solution) that regenerates the dye once it has injected photo-generated electrons into the oxide, and a counter electrode. This liquid component, in which the working electrode is embedded, is compatible with only a small set of known molecules, and the number of efficient dyes is small. A combination of these factors has hampered the development of new DSSCs. As an alternative to new chemistries, photonic elements that enhance the optical response have been studies as an approach to enhance the efficiency of DSSC, primarily with the goal of enhancing the absorption of the red part of the solar spectrum. Among these elements, the most successful to date are incoherent scattering layers. These are films that are several micrometers thick and composed of large TiO_2 particles (with a diameter of the order of the wavelength of visible light) that increase the effective optical-path length within the cell.[115,116] 3D photonic crystals, such as titania inverse opals (Fig. 17a) are also good candidates for consideration as components of a DSSC. In such structures, air voids are periodically arranged in the oxide matrix. The high level of porosity enables the electrolyte to be in close contact with the maximum area of the working electrode, yet the titania remains interconnected, which is critical for charge transport. The first inverse opal coupled to a DSSC was fabricated by Mallouk.[117] A 26% increase in photocurrent was measured in those cells, as compared to a reference DSSC, although the reasons for the enhancement remained unclear. Mihi and Miguez subsequently provided insight into the origin of this enhancement; the photocurrent enhancement was attributed to the optical coupling of the titania layer and the photonic crystal.[118] This coupling results in standing waves in the active layer, which enhances the absorption of light by the dye at those wavelengths. This phenomenon takes place at wavelengths lying within the photonic pseudo gap. Through the use of this effect, it may be possible to tune the spectral range where the absorption enhancement is going to occur by appropriately selecting the crystal lattice parameter. Experimental evidence of this phenomenon can be found in the literature.[119,120] Photonic-crystal-based optical coupling has also been successfully studied in silicon solar cells, where a colloidal crystal was coupled to a silicon solar cell, resulting in a higher photocurrent amplification than when using a common metallic mirror.[121]

The 3D photonic crystals coupled to solar cells discussed above exploit the photonic pseudo-bandgap that appear as a consequence of the diffraction from the (111) planes of the fcc structure. The same effect could be realized using one-dimensional structures, thus avoiding the difficulties of the

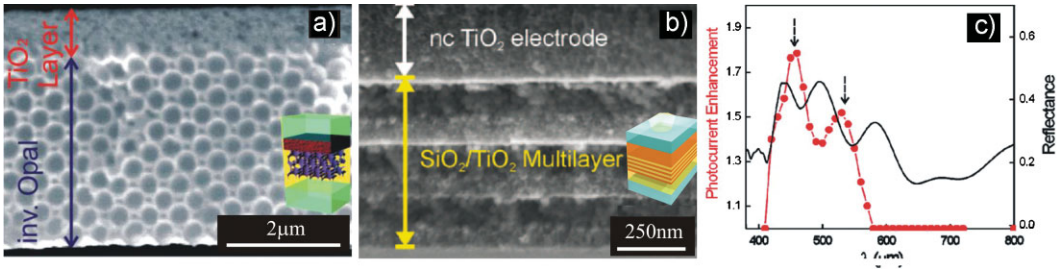

Figure 17. a) SEM images corresponding to nanoparticle TiO_2-based electrodes coupled to a 3D inverse titania photonic crystal. Adapted with permission from [119]. Copyright 2009, American Chemical Society. b) A 1D porous Bragg reflector fabricated from alternating colloidal silica and titania layers, respectively. The inset shows a schematic image of the PV device. c) Reflectance spectrum (black line) obtained from the solar cell and 1D structure depicted in (b) and the measured photocurrent enhancement (red line). Images (b,c) adapted with permission from [122]. Copyright 2009, American Chemical Society.

processing a three-dimensional structure, however at least for DSSCs, the structure must be porous in order to let the electrolyte reach the electrode. Miguez recently achieved this goal, where porous distributed Bragg reflectors (DBR) were made by alternate spin coating of titania and silica colloids (Fig. 17b). Such DBR's exhibit both high optical quality and can be easily formed. When such structures were combined with standard DSSC (Fig. 17c) the optical resonances discussed above[122] were used to enhance the external quantum efficiency of the cell, increasing the overall efficiency by up to 30%.[123]

4.3.2. Fabrication of Tailored Absorbing Layers

Traditionally, decreasing the cost of the silicon and other absorber materials commonly used for solar cells have unfortunately been coupled to reductions in the crystallinity and purity of the material and thus efficiency. Examples of low-cost, low-efficiency solar cells include those based on polycrystalline or amorphous silicon, nanoparticles, and polycrystalline compound semiconductors. Over the last years, several exciting new directions have been taken to decouple the relationship between cost and efficiency. New processing technologies discovered by Rogers and co-workers[124–131] are enabling silicon wafers to be processed into small units that can be reassembled into PV modules that exhibit novel advantages never seen before in silicon solar cells, including flexibility and transparency.[131] As an added value, the silicon is being used much more efficiently than ever before. It has now been demonstrated that crystalline silicon can be tailored in many shapes including rectangles and spheres, and these structures have even been transferred to glass substrates, demonstrating the generality of this approach.[132–134] In the silicon solar micro-cell (μ-cell) work of Rogers, starting with monocrystalline silicon, μ-cells several millimeters in length and down to hundreds of nanometers thick were formed by means of specialized anisotropic etching techniques. By using elastomeric stamps [poly(dimethylsiloxane); PDMS] for transfer-printed assembly, μ-cells fabricated in this way were subsequently transfer-printed onto polymeric substrates,[131] resulting in flexible silicon solar modules that can be bent several times to a curvature radius of 4.9 mm with little change in their electrical properties. An additional benefit of transfer-printed μ-cells is the ability, through carefully engineered PDMS stamps, to vary the transparency of the resulting silicon solar modules, which resulted in transparencies ranging from a few percent up to 70%, as determined by the spacing between μ-cells. The efficiency of these μ-cells can be as high as 13% when coupled with a diffusive backside reflector and further reduction in the amount of silicon usage is possible by implementing low-profile microlens concentrators. A very powerful element of this fabrication approach and assembly via PDMS stamps is that expensive, but high-efficiency PV materials such as GaAs and other III–V solar materials can be utilized at very low cost since the thin (1–3-μm-thick) single-crystal elements are transfer-printed onto low-cost substrates, requiring very little GaAs per unit area. Through the use of microconcentrators, only low-fill fractions of the μ-cells are required for efficient light harvesting, further reducing the usage of the expensive semiconductor. Collectively, the results show that the materials, design layout, and performance of these silicon solar μ-cells can result in the fabrication of unusual Si PV modules, in ways that cannot be achieved with conventional wafer-based PV technologies.

For individual μ-cells to form an effective solar cell module there is need for efficient methods to wire them together to yield large-area and high-power solar cells. To maintain the low cost, traditional methods of wiring, such as wire bonding, which might fracture the very thin microcells, are not appropriate. As an alternative, the direct ink writing technique developed by Lewis exhibits the necessary 3D spatial resolution to generate good electrical connections between the μ-cells and, more importantly, can create spanning silver wires which connect the μ-cells without risk of forming short circuits in a high-throughput fashion.[135]

4.3.3. Modifying of the Spectral Distribution: Thermophotovoltaics

Assuming no electrical losses, the power conversion efficiency of the ideal two-band photoconverter is a function of its bandgap energy, the power, and the spectral distribution of the incoming radiation. Under the standard AM 1.5 solar irradiance, the maximum efficiency that can be extracted from this device is around 31% in absence of light concentration, using a material with the optimum bandgap located at 1.4 eV. This limit, imposed by thermodynamics (the Shockley–Queisser limit), can be overcome if multiple bandgaps (multiple absorber layers) are integrated into the same device, however at considerable cost.[136] At least theoretically, a thermophotovoltaic (TPV)-based solar cell could far exceed the Shockley–Queisser limit. Under ideal conditions, a single-junction TPV cell can reach 85% efficiency.[137] However, this requires a perfect material, which converts incident radiance with 100% efficiency to radiation that is tailored to be just greater in energy than the bandgap of the absorber. This material, an intermediate layer between the solar radiance and the PV cell, needs to be a perfect absorber over the entire solar spectrum and a narrow-band emitter. As the intermediate layer absorbs the sunlight it heats up and starts to glow; this thermal radiation then needs to be concentrated onto the PV cell (Fig. 18).[137] For there to be a reasonable intensity of the emission, it will be necessary that the intermediate layers

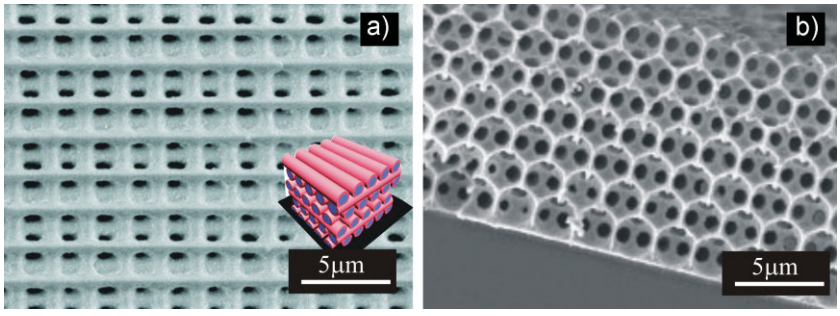

Figure 18. SEM images corresponding to 3D metallic photonic crystals with TPV applications. a) Tungsten woodpile structure as shown schematically in the inset. Reproduced with permission from [156]. Copyright 2008, American Chemical Society. b) Nickel inverse opal with 13% filling fraction. Adapted from [141].

reach temperatures exceeding 1000 °C, and thus only a limited subset of materials, such as tungsten, for example, may be possible candidates. Metallic photonic crystals are an interesting candidate to serve as the intermediate layer due to the possibility of tuning their emission and absorption properties through structure.[138] Photonic-crystal-based absorption phenomena have been observed in 3D tungsten structures; however, in the early work, the structures where fabricated via lithographic approaches, limiting their viability.[139–141] More recently, Norris fabricated tungsten and molybdenum woodpile structures (Fig. 18a), whose thermal emission at 650 °C is expected to match the absorption of InGaAsSb cells with a potential maximum efficiency of 32%. However, the study of these structures at higher temperatures could not be performed due to a structural instability of the materials at higher temperatures.

Braun controlled the optical properties of 3D nickel photonic crystals by regulating the filling fraction of metal in an inverse opal structure by a combination of electrodeposition and etching.[141] These inverse opal structures with as little as 5% nickel by volume (Fig. 18b), survived up to 450 °C as formed and up to 800 °C once the nickel was conformally coated with Al_2O_3 via atomic layer deposition. Although the preliminary work has been promising, considerable work remains for TPV devices to become reality. A combination of complex 3D photonic crystals, such as those formed via holographic techniques, and new processing approaches for materials with high temperature stability are clearly required.

4.4. Photonic-Crystal Sensors

One interesting application for photonic crystals is in the field of sensing. Typically, photonic-crystal sensors are functionalized such that in the presence of an analyte, the structure or optical properties of the photonic crystal change, leading to a change in its optical response. Optical biosensing typically falls into one of two categories: detection of fluorescently labeled molecules, or detection of label-free molecules. A review on the sensing of unlabeled molecules has recently been published.[142] This mode of detection is generally desirable, as fluorescent labeling is not necessary, reducing the chance of inflicting harm on the biological systems involved. Sensing systems including surface plasmon resonance devices, interferometers, optical fibers, and photonic crystals have all been applied to this important problem. Photonic crystals are of particular interest because of the potential for direct optical readout. One, two, and three-dimensional photonic crystals have been used to detect various substances including (but not limited to) creatinine, ethanol, various proteins, glucose, metallic cations, nerve agents, and other liquid- and vapor-phase materials.[142]

A 1D photonic crystal, a simple grating, can for example be molded into a sol–gel precursor spun onto a flexible plastic substrate. In recent work reported by Cunningham and co-workers, the mold was created using a PDMS replica of a grating etched into a silicon master. Following conversion of the sol–gel layer to low-index, porous SiO_2, the biosensor was completed by adding a high-dielectric layer to the top surface (Fig. 19).[143] When illuminated with white light at normal incidence, the structure reflects a narrow frequency band with near-100% efficiency. A receptor for the protein lactoferrin was

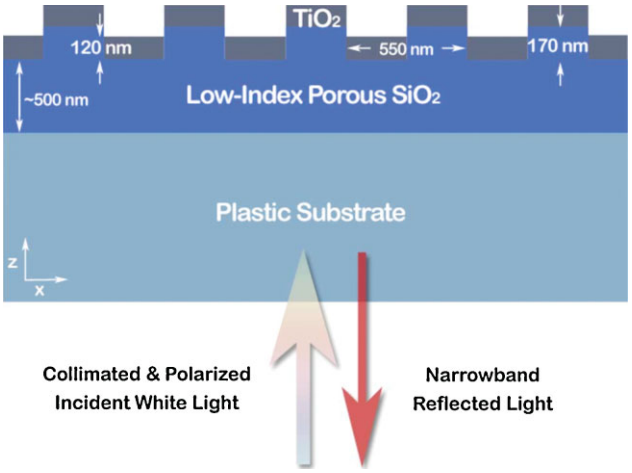

Figure 19. 1D photonic-crystal biosensor on a flexible plastic substrate. Reproduced with permission from [143]. Copyright 2008, Institute of Electrical and Electronics Engineers.

immobilized to the surface of the device; lactoferrin binding events could be detected by a positive shift in the wavelength of the reflectance peak.[143] In the simple case of porous 1D photonic structures, analytes can condense from the gas phase into the pores of the photonic crystal, changing the refractive index of these layers. The change in the dielectric contrast induces a modification in the reflectance, which can be related to the quantity of condensed analyte.[144–146]

In a 2D photonic crystal it is possible to localize the electric field in the air regions of the structure. When a linear or point defect is incorporated into the crystal, local changes in refractive index contrast caused by molecular binding events in the defect region, strongly modulate the optical properties of the defect.[147,148] A few years ago, Lee and Fauchet extended the usefulness of these devices beyond just detection techniques. In 2007, they demonstrated the ability to measure the diameter of a protein bound to a microcavity structure.[147]

The most-popular 3D photonic-crystal sensors are based on hydrogels. Two common configurations are used: hydrogels containing an embedded colloidal crystal array[149] and inverse opal hydrogels.[150] Hydrogels can be designed to be sensitive to molecular binding events, pH, relative humidity, temperature, and solvent quality, opening the potential for a diverse array of applications for hydrogel-based photonic-crystal sensors. Hydrogels containing an embedded colloidal crystal array function by undergoing volumetric changes as a result of some environmental change. Analyte-triggered swelling increases the lattice constant of the embedded colloidal array, which red shifts the optical response. This concept is quite general and only requires the hydrogel to be designed to swell in response to some event.

Inverse opal hydrogels function via a similar process, however, a sacrificial colloidal-crystal template, rather than embedded colloidal particles, is used to create the periodic hydrogel structure.[150] In response to a chemical stimuli, the hydrogel material swells causing the inverse opal structure to expand (resulting in a red shift). Because of the porous nature of the templated structures, the kinetics of the response can be quite rapid, relative to the colloidal-crystal-array-based systems.

4.5. Future Directions: Active Photonic Structures

Although the use of photonic crystals in PV devices has been extensively studied, their application has primarily been to serve as a dielectric stack reflective element or a diffractive element. These limited uses leave many of the most-interesting properties of photonic crystals as of yet unexploited, such as the use of photonic bands with associated high density of states to increase the effective absorption coefficient. Another area where photonic crystals can make improvements to PV devices is through their frequency-dependent scattering strength that can be used to enhance photon absorption.

Through non-traditional, large-area, semiconductor processing technologies based on soft lithography, entire new designs for low-cost, high-efficiency solar cells have been enabled. These approaches enable the fabrication of PV modules with unusual form factors, such as those composed of horizontally or vertically stacked μ-cells which have great potential for efficient light harvesting. Once this technology is coupled with the emerging capability of making electrical contacts in 3D at the micrometer scale, there is the potential to fabricate micrometer-scale multijunction PV cells without complicated and expensive semiconductor processing techniques. Such multijunction cells could achieve much higher efficiencies than single-junction cells without the normally associated costs of multijunction PV cells.

TPV light-harvesting strategies have exceptional theoretical potential; however, very significant challenges remain to realize such structures. Fundamentally, the emitter needs to withstand the high temperatures required for light emission and, at the same time, control the direction and frequency of this emission. Accomplishing this in a real material, which has to withstand temperatures exceeding 1000 °C, while maintaining its patterned structure on the submicromter scale, will be a challenge.

Photonic structures are becoming increasingly attractive for sensing applications, providing an optical response related to the detection of targeted molecules. In some cases, such as glucose sensing, photonic structures can be used to provide a noninvasive detection path. The materials chosen for these purposes are mostly hydrogels, which produce structures with a poor refractive-index contrast with aqueous media. Therefore, the development of high-index-contrast photonic-structure-based sensors would provide better optical detection upon changes in the structure. Also, photonic-based sensors can be exploited as an inexpensive and simple device, providing a path to real-time detection with the naked eye. These characteristics make photonic crystals excellent candidates for analytical probes in health diagnostics.

5. Electronic-Grade Photonic Crystals

Semiconducting laser performance and efficiency is significantly degraded by undesired spontaneous emission.[151] Photonic crystals show great promise to inhibit this spontaneous emission and thus increase the efficiency of a semiconductor laser. Devices such as VCSELs utilize 1D photonic crystals or distributed Bragg reflectors. VCSELs comprised of semiconductor-grade materials can be easily fabricated. Lasers using 2D photonic crystals can also be fabricated from semiconductor-grade materials, with only slightly greater difficulty. However, to achieve complete spontaneous-emission inhibition, 3D photonic crystals will be required. Despite the dramatic strides to date, all the fabrication methods for 3D photonic crystals containing embedded defects lack the ability to produce structures that are suitable for electrically pumped light emission due to the fact that they are not fabricated from "electronic-grade" materials. The photonic crystals are formed from materials that are amorphous or polycrystalline and thus are unlikely to serve as effective materials for electrically pumped emission. If cPBG materials are to be used for applications including low-threshold lasers, LEDs, solar cells, and ultimately all optical circuitry, high-quality semiconducting materials will be required to achieve optimal device performance and efficiency. The closest results to date are woodpile structures that have been fabricated via layer-by-layer stacking of single-crystal silicon or III–IV materials.[8] However, the interface between the layers is of unknown electrical quality, which will increase both nonradiative decay and the overall resistance of the structure. Recently, crystalline silicon inverse opals were fabricated via CVD and subsequent thermal annealing.[152] Electrical properties acceptable for device applications were obtained following hydrogen-plasma passivation to reduce the number of Si dangling bonds (electronic trap sites); however, silicon inherently is not an efficient emitter. Also recently, Noda and co-workers fabricated a single-crystal silicon 3D photonic crystal by a double-angle, deep-etching method.[153] Etching was accomplished using reactive ion etching at angles ±45° with respect to the sample surface. The structures formed resemble 3D woodpile photonic crystals, as can be observed from the schematic representations and the SEM image in Figure 20a and 20b,

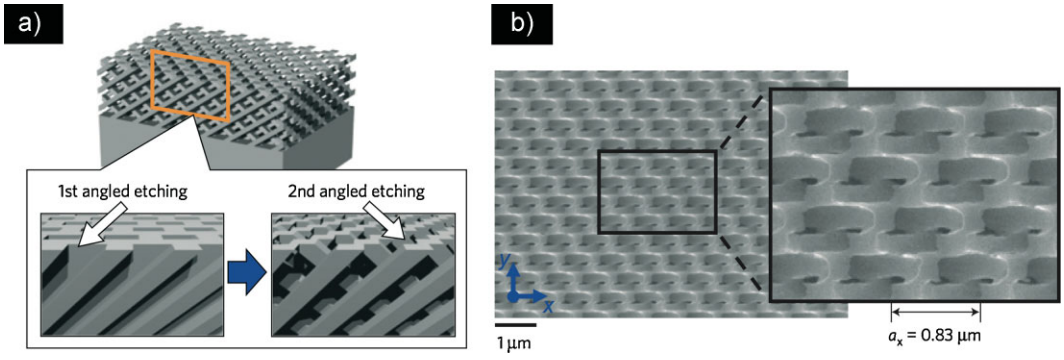

Figure 20. a) Schematic representation of the double-angle etching procedure used to fabricate 3D photonic crystals. b) Top view of the resultant structures fabricated using reactive ion etching. Reproduced with permission from [153]. Copyright 2009, Macmillan Publishers Ltd.

respectively. This is the first account of high-optical-quality photonic crystals fabricated using an etching procedure. To date, however, electrically driven emission from photonic crystals has not been demonstrated. Perhaps some combination of interference lithography, improved high-temperature photoresists, and novel materials-deposition strategies will enable realization of these goals.

6. Conclusions and Future Directions

Over the last few years, great strides have been accomplished in the fabrication and modeling of multidimensional architectures for advanced photonic applications, yet it is also clear that considerable work remains to be carried out to fully unleash their technological potential. Already, new low-cost, high-efficiency solar cells, large-area 3D photonic crystals, unique metamaterials, and powerful chemical and biological sensors have been realized. However, the subset of materials and structures that can be fabricated remains limited. Ideally, one would be able to pattern any material with any periodic or aperiodic multidimensional structure as required. New and emerging simulation tools, including topology optimization and genetic algorithms, motivate the need for further advances in 3D fabrication. Although the subject of this Review has been on optically active structures, materials exhibiting complex multidimensional architectures may find application in many more diverse settings, including electrochemical energy storage, separation processes, fuel cells, and catalysis.

Acknowledgements

The authors thank the U.S. Department of Energy, Division of Materials Sciences under Award No. DE-FG02-07ER46471, through the Frederick Seitz Materials Research Laboratory at the University of Illinois at Urbana-Champaign for supporting the work of the authors' laboratories reported in this Review. A.M. gratefully acknowledges support of a Beckman Institute Postdoctoral Fellowship.

Received: November 30, 2009
Published online: February 1, 2010

[1] *Photonic Crystals: Physics, Fabrication, and Applications*, (Eds: K. Inoue, K. Ohtaka), Springer, Berlin **2004**.
[2] E. C. Nelson, P. V. Braun, *Nat. Photonics* **2008**, *2*, 650.
[3] E. Yablonovitch, *Phys. Rev. Lett.* **1987**, *58*, 2059.
[4] R. D. Meade, A. Devenyi, J. D. Joannopoulos, O. L. Alerhand, D. A. Smith, K. Kash, *J. Appl. Phys.* **1994**, *75*, 4753.
[5] S. H. Fan, J. N. Winn, A. Devenyi, J. C. Chen, R. D. Meade, J. D. Joannopoulos, *J. Opt. Soc. Am. B* **1995**, *12*, 1267.
[6] A. Mekis, J. C. Chen, I. Kurland, S. H. Fan, P. R. Villeneuve, J. D. Joannopoulos, *Phys. Rev. Lett.* **1996**, *77*, 3787.
[7] S. John, *Phys. Rev. Lett.* **1987**, *58*, 2486.
[8] S. Noda, K. Tomoda, N. Yamamoto, A. Chutinan, *Science* **2000**, *289*, 604.
[9] E. Yablonovitch, T. J. Gmitter, R. D. Meade, A. M. Rappe, K. D. Brommer, J. D. Joannopoulos, *Phys. Rev. Lett.* **1991**, *67*, 3380.
[10] A. Arsenault, F. Fleischhaker, G. von Freymann, V. Kitaev, H. Miguez, A. Mihi, N. Tetreault, E. Vekris, I. Manners, S. Aitchison, D. Perovic, G. A. Ozin, *Adv. Mater.* **2006**, *18*, 2779.
[11] L. F. Shen, Z. Ye, S. He, *Phys. Rev. B* **2003**, *68*.
[12] A. Gondarenko, S. Preble, J. Robinson, L. Chen, H. Lipson, M. Lipson, *Phys. Rev. Lett.* **2006**, *96*.
[13] A. Hakansson, J. Sanchez-Dehesa, *Opt. Express* **2005**, *13*, 5440.
[14] A. Hakansson, J. Sanchez-Dehesa, L. Sanchis, *IEEE J. Sel. Areas Commun.* **2005**, *23*, 1365.
[15] J. W. Rinne, P. Wiltzius, *Opt. Express* **2006**, *14*, 9909.
[16] J. W. Rinne, Ph. D. Thesis, University of Illinois at Urbana-Champaign **2009**.
[17] W. R. Frei, H. T. Johnson, *Phys. Rev. B* **2004**, 70.
[18] J. S. Jensen, O. Sigmund, *Appl. Phys. Lett.* **2004**, *84*, 2022.
[19] W. R. Frei, D. A. Tortorelli, H. T. Johnson, *Appl. Phys. Lett.* **2005**, *86*, 111114.
[20] W. R. Frei, H. T. Johnson, K. D. Choquette, *J. Appl. Phys.* **2008**, *103*, 3410.
[21] W. R. Frei, D. A. Tortorelli, H. T. Johnson, *Opt. Lett.* **2007**, *32*, 77.
[22] E. Hetch, *Optics*, Addison Wesley, Reading, Mass., USA **2001**.
[23] G. A. Ozin, K. Hou, B. V. Lotsch, L. Cademartiri, D. P. Puzzo, F. Scotognella, A. Ghadimi, J. Thomson, *Mater. Today* **2009**, *12*, 12.
[24] L. D. Bonifacio, B. V. Lotsch, D. P. Puzzo, F. Scotognella, G. A. Ozin, *Adv. Mater.* **2009**, *21*, 1641.
[25] S. Colodrero, M. Ocana, H. Miguez, *Langmuir* **2008**, *24*, 4430.
[26] D. P. Puzzo, L. D. Bonifacio, J. Oreopoulos, C. M. Yip, I. Manners, G. A. Ozin, *J. Mater. Chem.* **2009**, *19*, 3500.
[27] B. V. Lotsch, C. B. Knobbe, G. A. Ozin, *Small* **2009**, *5*, 1498.
[28] M. C. Fuertes, F. J. Lopez-Alcaraz, M. C. Marchi, H. E. Troiani, V. Luca, H. Miguez, G. Soler-Illia, *Adv. Funct. Mater.* **2007**, *17*, 1247.
[29] M. E. Calvo, S. Colodrero, T. C. Rojas, J. A. Anta, M. Ocana, H. Miguez, *Adv. Funct. Mater.* **2008**, *18*, 2708.
[30] C. Lopez, *Adv. Mater.* **2003**, *15*, 1679.
[31] P. Jiang, J. F. Bertone, K. S. Hwang, V. L. Colvin, *Chem. Mat.* **1999**, *11*, 2132.
[32] Y. N. Xia, B. Gates, Y. D. Yin, Y. Lu, *Adv. Mater.* **2000**, *12*, 693.
[33] Y. A. Vlasov, X. Z. Bo, J. C. Sturm, D. J. Norris, *Nature* **2001**, *414*, 289.
[34] N. Yamamoto, S. Noda, A. Chutinan, *Jpn. J. Appl. Phys., Part 2* **1998**, *37*, L1052.
[35] S. Y. Lin, J. G. Fleming, D. L. Hetherington, B. K. Smith, R. Biswas, K. M. Ho, M. M. Sigalas, W. Zubrzycki, S. R. Kurtz, J. Bur, *Nature* **1998**, *394*, 251.
[36] G. M. Gratson, F. Garcia-Santamaria, V. Lousse, M. J. Xu, S. H. Fan, J. A. Lewis, P. V. Braun, *Adv. Mater.* **2006**, *18*, 461.
[37] H. B. Sun, S. Matsuo, H. Misawa, *Appl. Phys. Lett.* **1999**, *74*, 786.
[38] N. Tetreault, G. von Freymann, M. Deubel, M. Hermatschweiler, F. Perez-Willard, S. John, M. Wegener, G. A. Ozin, *Adv. Mater.* **2006**, *18*, 457.
[39] V. Berger, O. Gauthier-Lafaye, E. Costard, *J. Appl. Phys.* **1997**, *82*, 60.
[40] S. Jeon, J. U. Park, R. Cirelli, S. Yang, C. E. Heitzman, P. V. Braun, P. J. A. Kenis, J. A. Rogers, *Proc. Natl. Acad. Sci. USA* **2004**, *101*, 12428.
[41] P. V. Braun, S. A. Rinne, F. Garcia-Santamaria, *Adv. Mater.* **2006**, *18*, 2665.
[42] A. P. Philipse, *J. Mater. Sci. Lett.* **1989**, *8*, 1371.
[43] S. A. Rinne, F. Garcia-Santamaria, P. V. Braun, *Nat. Photonics* **2008**, *2*, 52.
[44] J. S. King, E. Graugnard, C. J. Summers, *Adv. Mater.* **2005**, *17*, 1010.
[45] R. M. Almeida, S. Portal, *Curr. Opin. Solid State Mater. Sci.* **2003**, *7*, 151.
[46] J. I. L. Chen, G. von Freymann, S. Y. Choi, V. Kitaev, G. A. Ozin, *Adv. Mater.* **2006**, *18*, 1915.
[47] P. V. Braun, P. Wiltzius, *Nature* **1999**, *402*, 603.
[48] O. D. Velev, T. A. Jede, R. F. Lobo, A. M. Lenhoff, *Nature* **1997**, *389*, 447.
[49] M. Ibisate, D. Golmayo, C. Lopez, *Adv. Mater.* **2009**, *21*, 2899.
[50] F. Ramiro-Manzano, F. Meseguer, E. Bonet, I. Rodriguez, *Phys. Rev. Lett.* **2006**, *97*.
[51] F. Garcia-Santamaria, H. T. Miyazaki, A. Urquia, M. Ibisate, M. Belmonte, N. Shinya, F. Meseguer, C. Lopez, *Adv. Mater.* **2002**, *14*, 1144.
[52] D. C. Benito, D. M. Carberry, S. H. Simpson, G. M. Gibson, M. J. Padgett, J. G. Rarity, M. J. Miles, S. Hanna, *Opt. Express* **2008**, *16*, 13005.
[53] A. P. Hynninen, J. H. J. Thijssen, E. C. M. Vermolen, M. Dijkstra, A. Van Blaaderen, *Nat. Mater.* **2007**, *6*, 202.

[54] P. D. Garcia, R. Sapienza, A. Blanco, C. Lopez, *Adv. Mater.* **2007**, *19*, 2597.
[55] R. Sapienza, P. D. Garcia, J. Bertolotti, M. D. Martin, A. Blanco, L. Vina, C. Lopez, D. S. Wiersma, *Phys. Rev. Lett.* **2007**, *99*.
[56] S. Gottardo, R. Sapienza, P. D. Garcia, A. Blanco, D. S. Wiersma, C. Lopez, *Nat. Photonics* **2008**, *2*, 429.
[57] C. N. LaFratta, J. T. Fourkas, T. Baldacchini, R. A. Farrer, *Angew. Chem. Int. Ed.* **2007**, *46*, 6238.
[58] L. J. Li, J. T. Fourkas, *Mater. Today* **2007**, *10*, 30.
[59] E. B. Duoss, M. Twardowski, J. A. Lewis, *Adv. Mater.* **2007**, *19*, 3485.
[60] G. M. Gratson, J. A. Lewis, *Langmuir* **2005**, *21*, 457.
[61] G. M. Gratson, M. J. Xu, J. A. Lewis, *Nature* **2004**, *428*, 386.
[62] J. A. Lewis, *Adv. Funct. Mater.* **2006**, *16*, 2193.
[63] F. Garcia-Santamaria, M. J. Xu, V. Lousse, S. H. Fan, P. V. Braun, J. A. Lewis, *Adv. Mater.* **2007**, *19*, 1567.
[64] R. A. Barry, R. F. Shepherd, J. N. Hanson, R. G. Nuzzo, P. Wiltzius, J. A. Lewis, *Adv. Mater.* **2009**, *21*, 2407.
[65] M. Campbell, D. N. Sharp, M. T. Harrison, R. G. Denning, A. J. Turberfield, *Nature* **2000**, *404*, 53.
[66] Y. C. Chen, J. B. Geddes, J. T. Lee, P. V. Braun, P. Wiltzius, *Appl. Phys. Lett.* **2007**, *91*, 241103.
[67] D. Shir, H. W. Liao, S. Jeon, D. Xiao, H. T. Johnson, G. R. Bogart, K. H. A. Bogart, J. A. Rogers, *Nano Lett.* **2008**, *8*, 2236.
[68] D. Shir, E. C. Nelson, Y. C. Chen, A. Brzezinski, H. Liao, P. V. Braun, P. Wiltzius, K. H. A. Bogart, J. A. Rogers, *Appl. Phys. Lett.* **2009**, *94*, 011101.
[69] S. Jeon, Y. S. Nam, D. J. L. Shir, J. A. Rogers, A. Hamza, *Appl. Phys. Lett.* **2006**, *89*, 253101.
[70] Y. S. Nam, S. Jeon, D. J. L. Shir, A. Hamza, J. A. Rogers, *Appl. Optics* **2007**, *46*, 6350.
[71] S. Jeon, V. Malyarchuk, J. A. Rogers, G. P. Wiederrecht, *Opt. Express* **2006**, *14*, 2300.
[72] M. C. George, E. C. Nelson, J. A. Rogers, P. V. Braun, *Angew. Chem. Int. Ed.* **2009**, *48*, 144.
[73] V. G. Veselago, *Sov. Phys. Uspekhi* **1968**, *10*, 509.
[74] R. A. Shelby, D. R. Smith, S. Schultz, *Science* **2001**, *292*, 77.
[75] D. R. Smith, W. J. Padilla, D. C. Vier, S. C. Nemat-Nasser, S. Schultz, *Phys. Rev. Lett.* **2000**, *84*, 4184.
[76] C. M. Soukoulis, M. Kafesaki, E. N. Economou, *Adv. Mater.* **2006**, *18*, 1941.
[77] C. Luo, S. G. Johnson, J. D. Joannopoulos, J. B. Pendry, *Phys. Rev. B* **2002**, *65*, 201104.
[78] P. V. Parimi, W. T. Lu, P. Vodo, J. Sokoloff, J. S. Derov, S. Sridhar, *Phys. Rev. Lett.* **2004**, *92*, 127401.
[79] J. B. Pendry, *Phys. Rev. Lett.* **2000**, *85*, 3966.
[80] E. Cubukcu, K. Aydin, E. Ozbay, S. Foteinopolou, C. M. Soukoulis, *Phys. Rev. Lett.* **2003**, *91*, 207401.
[81] K. Ren, Z. Y. Li, X. B. Ren, S. Feng, B. Y. Cheng, D. Z. Zhang, *Phys. Rev. B* **2007**, *75*, 115108.
[82] W. S. Cai, U. K. Chettiar, A. V. Kildishev, V. M. Shalaev, *Nat. Photonics* **2007**, *1*, 224.
[83] U. Leonhardt, *Science* **2006**, *312*, 1777.
[84] J. B. Pendry, D. Schurig, D. R. Smith, *Science* **2006**, *312*, 1780.
[85] D. Schurig, J. J. Mock, B. J. Justice, S. A. Cummer, J. B. Pendry, A. F. Starr, D. R. Smith, *Science* **2006**, *314*, 977.
[86] S. Guenneau, S. A. Ramakrishna, S. Enoch, S. Chakrabarti, G. Tayeb, B. Gralak, *Photonics Nanostruct. Fundam. Appl.* **2007**, *5*, 63.
[87] O. Vanbesien, N. Fabre, X. Melique, D. Lippens, *Appl. Optics* **2008**, *47*, 1358.
[88] D. Xiao, H. T. Johnson, *Opt. Lett.* **2008**, *33*, 860.
[89] J. Valentine, J. Li, T. Zentgraf, G. Bartal, X. Zhang, *Nat. Mater.* **2009**, *8*, 568.
[90] J. S. Li, J. B. Pendry, *Phys. Rev. Lett.* **2008**, *101*, 203901.
[91] W. M. Lee, S. A. Pruzinsky, P. V. Braun, *Adv. Mater.* **2002**, *14*, 271.
[92] V. Ramanan, E. Nelson, A. Brzezinski, P. V. Braun, P. Wiltzius, *Appl. Phys. Lett.* **2008**, *92*, 173304.
[93] H. G. Park, C. J. Barrelet, Y. N. Wu, B. Z. Tian, F. Qian, C. M. Lieber, *Nat. Photonics* **2008**, *2*, 622.
[94] E. C. Nelson, F. Garcia-Santamaria, P. V. Braun, *Adv. Funct. Mater.* **2008**, *18*, 1983.
[95] M. Okano, A. Chutinan, S. Noda, *Phys. Rev. B* **2002**, 66.
[96] O. Painter, R. K. Lee, A. Scherer, A. Yariv, J. D. O'Brien, P. D. Dapkus, I. Kim, *Science* **1999**, *284*, 1819.
[97] A. J. Danner, J. J. Raftery, N. Yokouchi, K. D. Choquette, *Appl. Phys. Lett.* **2004**, *84*, 1031.
[98] N. Yokouchi, A. J. Danner, K. D. Choquette, *IEEE J. Sel. Topics Quantum Electron.* **2003**, *9*, 1439.
[99] H. Y. Ryu, M. Notomi, Y. H. Lee, *Appl. Phys. Lett.* **2003**, *83*, 4294.
[100] K. Aoki, D. Guimard, M. Nishioka, M. Nomura, S. Iwamoto, Y. Arakawa, *Nat. Photonics* **2008**, *2*, 688.
[101] A. Tandaechanurat, S. Ishida, K. Aoki, D. Guimard, M. Nomura, S. Iwamoto, Y. Arakawa, *Appl. Phys. Lett.* **2009**, *94*, 171115.
[102] S. Noda, M. Fujita, *Nat. Photonics* **2009**, *3*, 129.
[103] Y. K. Ee, R. A. Arif, N. Tansu, P. Kumnorkaew, J. F. Gilchrist, *Appl. Phys. Lett.* **2007**, *91*, 221107.
[104] H. Ichikawa, T. Baba, *Appl. Phys. Lett.* **2004**, *84*, 457.
[105] K. McGroddy, A. David, E. Matioli, M. Iza, S. Nakamura, S. DenBaars, J. S. Speck, C. Weisbuch, E. L. Hu, *Appl. Phys. Lett.* **2008**, *93*, 103502.
[106] J. J. Wierer, A. David, M. M. Megens, *Nat. Photonics* **2009**, *3*, 163.
[107] H. Huang, C. H. Lin, C. C. Yu, C. H. Chiu, C. F. Lai, H. C. Kuo, K. M. Leung, T. C. Lu, S. C. Wang, B. D. Lee, *Nanotechnology* **2008**, *19*, 185301.
[108] M. A. Green, K. Emery, Y. Hishikawa, W. Warta, *Prog. Photovoltaics* **2009**, *17*, 85.
[109] H. W. Deckman, C. R. Wronski, H. Witzke, E. Yablonovitch, *Appl. Phys. Lett.* **1983**, *42*, 968.
[110] M. Florescu, H. Lee, I. Puscasu, M. Pralle, L. Florescu, D. Z. Ting, J. P. Dowling, *Sol. Energy Mater. Sol. Cells* **2007**, *91*, 1599.
[111] P. Bermel, C. Luo, L. Zeng, L. C. Kimerling, J. D. Joannopoulos, *Opt. Express* **2007**, *15*, 16986.
[112] G. von Freymann, W. Koch, D. C. Meisel, M. Wegener, M. Diem, A. Garcia-Martin, S. Pereira, K. Busch, J. Schilling, R. B. Wehrspohn, U. Gosele, *Appl. Phys. Lett.* **2003**, *83*, 614.
[113] D. Y. Zhou, R. Biswas, *J. Appl. Phys.* **2008**, *103*, 093102.
[114] B. Oregan, M. Gratzel, *Nature* **1991**, *353*, 737.
[115] J. Ferber, J. Luther, *Sol. Energy Mater. Sol. Cells* **1998**, *54*, 265.
[116] G. Rothenberger, P. Comte, M. Gratzel, *Sol. Energy Mater. Sol. Cells* **1999**, *58*, 321.
[117] S. Nishimura, N. Abrams, B. A. Lewis, L. I. Halaoui, T. E. Mallouk, K. D. Benkstein, J. van de Lagemaat, A. J. Frank, *J. Am. Chem. Soc.* **2003**, *125*, 6306.
[118] A. Mihi, H. Miguez, *J. Phys. Chem. B* **2005**, *109*, 15968.
[119] A. Mihi, M. E. Calvo, J. A. Anta, H. Miguez, *J. Phys. Chem. C* **2008**, *112*, 13.
[120] S. H. A. Lee, N. M. Abrams, P. G. Hoertz, G. D. Barber, L. I. Halaoui, T. E. Mallouk, *J. Phys. Chem. B* **2008**, *112*, 14415.
[121] P. G. O'Brien, N. P. Kherani, A. Chutinan, G. A. Ozin, S. John, S. Zukotynski, *Adv. Mater.* **2008**, *20*, 1577.
[122] S. Colodrero, A. Mihi, J. A. Anta, M. Ocana, H. Miguez, *J. Phys. Chem. C* **2009**, *113*, 1150.
[123] S. Colodrero, A. Mihi, L. Haggman, M. Ocana, G. Boschloo, A. Hagfeldt, H. Miguez, *Adv. Mater.* **2009**, *21*, 764.
[124] J. H. Ahn, H. S. Kim, K. J. Lee, S. Jeon, S. J. Kang, Y. G. Sun, R. G. Nuzzo, J. A. Rogers, *Science* **2006**, *314*, 1754.
[125] X. Feng, M. A. Meitl, A. M. Bowen, Y. Huang, R. G. Nuzzo, J. A. Rogers, *Langmuir* **2007**, *23*, 12555.
[126] S. H. Hur, D. Y. Khang, C. Kocabas, J. A. Rogers, *Appl. Phys. Lett.* **2004**, *85*, 5730.
[127] T. H. Kim, A. Carlson, J. H. Ahn, S. M. Won, S. D. Wang, Y. G. Huang, J. A. Rogers, *Appl. Phys. Lett.* **2009**, *94*, 189902.
[128] T. H. Kim, W. M. Choi, D. H. Kim, M. A. Meitl, E. Menard, H. Q. Jiang, J. A. Carlisle, J. A. Rogers, *Adv. Mater.* **2008**, *20*, 2171.

[129] M. A. Meitl, Z. T. Zhu, V. Kumar, K. J. Lee, X. Feng, Y. Y. Huang, I. Adesida, R. G. Nuzzo, J. A. Rogers, *Nat. Mater.* **2006**, *5*, 33.
[130] E. Menard, R. G. Nuzzo, J. A. Rogers, *Appl. Phys. Lett.* **2005**, *86*, 093507.
[131] J. Yoon, A. J. Baca, S. I. Park, P. Elvikis, J. B. Geddes, L. F. Li, R. H. Kim, J. L. Xiao, S. D. Wang, T. H. Kim, M. J. Motala, B. Y. Ahn, E. B. Duoss, J. A. Lewis, R. G. Nuzzo, P. M. Ferreira, Y. G. Huang, A. Rockett, J. A. Rogers, *Nat. Mater.* **2008**, *7*, 907.
[132] R. Brendel, R. B. Bergmann, P. Lolgen, M. Wolf, J. H. Werner, *Appl. Phys. Lett.* **1997**, *70*, 390.
[133] H. C. Ko, A. J. Baca, J. A. Rogers, *Nano Lett.* **2006**, *6*, 2318.
[134] A. J. Baca, M. A. Meitl, H. C. Ko, S. Mack, H. S. Kim, J. Y. Dong, P. M. Ferreira, J. A. Rogers, *Adv. Funct. Mater.* **2007**, *17*, 3051.
[135] B. Y. Ahn, E. B. Duoss, M. J. Motala, X. Y. Guo, S. I. Park, Y. J. Xiong, J. Yoon, R. G. Nuzzo, J. A. Rogers, J. A. Lewis, *Science* **2009**, *323*, 1590.
[136] J. Nelson, *The Physics of Solar Cells*, Imperial College Press, London **2003**.
[137] N. P. Harder, M. A. Green, *Semicond. Sci. Technol.* **2003**, *18*, S270.
[138] S. E. Han, A. Stein, D. J. Norris, *Phys. Rev. Lett.* **2007**, *99*, 053906.
[139] J. G. Fleming, S. Y. Lin, I. El-Kady, R. Biswas, K. M. Ho, *Nature* **2002**, *417*, 52.
[140] S. Y. Lin, J. Moreno, J. G. Fleming, *Appl. Phys. Lett.* **2003**, *83*, 380.
[141] X. D. Yu, Y. J. Lee, R. Furstenberg, J. O. White, P. V. Braun, *Adv. Mater.* **2007**, *19*, 1689.
[142] X. D. Fan, I. M. White, S. I. Shopoua, H. Y. Zhu, J. D. Suter, Y. Z. Sun, *Anal. Chim. Acta* **2008**, *620*, 8.
[143] I. D. Block, M. Pineda, C. J. Choi, B. T. Cunningham, *IEEE Sens. J.* **2008**, *8*, 1546.
[144] S. Colodrero, M. Ocana, A. R. Gonzalez-Elipe, H. Miguez, *Langmuir* **2008**, *24*, 9135.
[145] M. C. Fuertes, S. Colodrero, G. Lozano, A. R. Gonzalez-Elipe, D. Grosso, C. Boissiere, C. Sanchez, G. Soler-Illia, H. Miguez, *J. Phys. Chem. C* **2008**, *112*, 3157.
[146] J. Kobler, B. V. Lotsch, G. A. Ozin, T. Bein, *ACS Nano* **2009**, *3*, 1669.
[147] M. Lee, P. M. Fauchet, *Opt. Express* **2007**, *15*, 4530.
[148] N. Skivesen, A. Tetu, M. Kristensen, J. Kjems, L. H. Frandsen, P. I. Borel, *Opt. Express* **2007**, *15*, 3169.
[149] G. R. Hendrickson, L. A. Lyon, *Soft Matter* **2009**, *5*, 29.
[150] Y. J. Lee, C. E. Heitzman, W. R. Frei, H. T. Johnson, P. V. Braun, *J. Phys. Chem. B* **2006**, *110*, 19300.
[151] S. Noda, *Science* **2006**, *314*, 260.
[152] T. Suezaki, P. G. O'Brien, J. I. L. Chen, E. Loso, N. P. Kherani, G. A. Ozin, *Adv. Mater.* **2009**, *21*, 559.
[153] S. Takahashi, K. Suzuki, M. Okano, M. Imada, T. Nakamori, Y. Ota, K. I. Susumu, S. Noda, *Nat. Mater.* **2009**, *8*, 721.
[154] K. K. Seet, V. Mizeikis, S. Matsuo, S. Juodkazis, H. Misawa, *Adv. Mater.* **2005**, *17*, 541.
[155] A. Ledermann, L. Cademartiri, M. Hermatschweiler, C. Toninelli, G. A. Ozin, D. S. Wiersma, M. Wegener, G. von Freymann, *Nat. Mater.* **2006**, *5*, 942.
[156] P. Nagpal, S. E. Han, A. Stein, D. J. Norris, *Nano Lett.* **2008**, *8*, 3238.